Acceptance Study for the GlueX detector system

Joachim Kuhn , Curtis Meyer

Carnegie Mellon University
Department of Physics
5000 Forbes Ave.
Pittsburgh, PA 15213

3 September 2004

Abstract

We have carried out a study of the acceptance for the GlueX detector system. We show the acceptance as a function of the angles in the reference frames used for partial wave analysis (PWA) for several different final states populated from the decay of varying initial meson resonances. The resonances are produced by the interaction of a photon with a proton target and their masses and widths follow values predicted from flux tube model calculations. We will also present values for the acceptance of charged pions and for photons from the decay of neutral pions and eta mesons. A discussion on where events are lost in the detector will be presented as well.

1 Introduction

The main goal for the just recently approved GlueX experiment and detector system is to find evidence for exotic meson, that is states with quantum numbers of spin J, parity P and charge-conjugation C, J^{PC}, that cannot be produced by just a $q\bar{q}$ pair. In recent years analyses and theoretical calculations have shown that these exotic states are to a very high extent decaying into mesons with rather complicated decay patterns, involving multiple charged pions, charged Kaons and several photons. The signal for evidence of these states is usually extracted by performing a partial wave analysis (PWA). It is preferable for a detector searching for these states to have a high acceptance for all the above mentioned particles and also that there are no sudden variations in the variables used in the PWA. The goal of this study is to show that the expected acceptance with the current detector design is high for all the

particles in question. We here will concentrate on decays into pions and photons, since the design of the Cerenkov detector, which will distinguish between pions and Kaons, is not finalized at this point. A study of decays involving Kaons is therefore deferred to a later point.

2 Event generation

Events for this study were generated with a peripheral phase space distribution and isotropically distributed decay angles, using the program `genr8` [1]. The slope of the four-momentum distribution

$$\frac{d\sigma}{dt} \propto e^{-b|t|} \tag{1}$$

was fixed at $b = 5.0\ (\mathrm{GeV}/c)^2$, consistent with peripheral production of mesons and the photon beam energy was set to $E_\gamma = 9.0$ GeV. We chose final states according to the predicted strongest decay branches of the exotic states with quantum numbers $J^{PC} = 1^{-+}, 2^{+-}, 0^{+-}$, both for isospin $I = 0$ and $I = 1$ from calculations by P. Page, E. Swanson and A. Szczepaniak [2]. An overview over these decays can be found in Table 1. The breakup of the resonances is proceeding via successive two-body decays with Breit-Wigner mass distributions for the unstable intermediate states and isotropically distributed decay angles until the final state particles (charged pions and photons) are reached. The following is an example for a typical reaction and decay chain for a resonance X produced by the interaction of a photon beam with a proton target

$$\begin{aligned}
\gamma p &\to X^\circ p \\
&\quad X^\circ \to a_1^- \pi^+ \\
&\qquad a_1^- \to \rho^- \pi^\circ \quad , \quad \pi^\circ \to \gamma\gamma \\
&\qquad\quad \rho^- \to \pi^- \pi^\circ , \quad \pi^\circ \to \gamma\gamma
\end{aligned}$$

If available the masses and widths of the exotic mesons were matched to observed values, otherwise they were chosen in the range of the theoretical predictions. Table 2 gives an overview over all the decay chains and the values in this study.

For each topology 100 000 events were generated, which were then processed through the Hall D Monte Carlo program package, `HDFast`. The program contains the geometry of the detector system and events are accepted when all final state particles were "detected". Photons in the final state were required to be observed in either or both, the barrel calorimeter (BCAL) and the lead glass detector array (LGD) and the charged pions needed to generate at least 4 hits per track in the forward drift chambers (FDC) in order to not be lost.

	Isospin $I = 1$			*Isospin* $I = 0$		
	State	*Decay*	*Strength*	*State*	*Decay*	*Strength*
1^{-+}	π_1	$b_1(1235)\pi$	1	η_1	$\pi(1300)\pi$	1
		$f_1(1285)\pi$	$\frac{1}{4}$		$a_1(1260)\pi$	1
		$\rho(770)\pi$	$\frac{1}{4}$			
		$a_1(1260)\eta$	$\frac{1}{5}$			
2^{+-}	b_2	$a_1(1260)\pi$	1	h_2	$b_1(1235)\pi$	1
		$h_1(1170)\pi$	1		$\rho(770)\pi$	1
		$\omega(782)\pi$	$\frac{1}{2}$		$\omega(782)\eta$	$\frac{1}{10}$
		$a_2(1320)\pi$	$\frac{1}{4}$			
0^{+-}	b_0	$\pi(1300)\pi$	1	h_0	$b_1(1235)\pi$	1
		$h_1(1170)\pi$	$\frac{1}{5}$		$h_1(1170)\pi$	$\frac{1}{30}$

Table 1
Decay modes for exotic mesons as predicted from Ref [2]

#	*State*	*Mass*	*Width*	*Decay*
1	η_1	1800	300	$a_1(1260)^-\pi^+ \to [\rho^\circ\pi^-]\pi^+ \to [(\pi^+\pi^-)\pi^-]\pi^+$
2	η_1	1800	300	$a_1(1260)^-\pi^+ \to [\rho^-\pi^\circ]\pi^+ \to [(\pi^-\pi^\circ)\pi^\circ]\pi^+$
3	π_1°	1700	400	$f_1(1285)\pi^\circ \to [a_0(980)\pi^\circ]\pi^\circ \to [(\pi^\circ\eta)\pi^\circ]\pi^\circ$
4	π_1°	1700	400	$a_1(1260)^\circ\eta \to [\rho(770)^+\pi^-]\eta \to [(\pi^+\pi^\circ)\pi^-]\eta$
5	b_2^+	2000	300	$a_1(1260)^+\pi^\circ \to [\rho(770)^+\pi^\circ]\pi^\circ \to [(\pi^+\pi^\circ)\pi^\circ]\pi^\circ$
6	π_1^+	1700	400	$b_1(1235)^+\pi^\circ \to [\omega(782)\pi^+]\pi^\circ \to [(\pi^+\pi^-\pi^\circ)\pi^+]\pi^\circ$
7	h_2	2000	300	$b_1(1235)^-\pi^+ \to [\omega(782)\pi^-]\pi^+ \to [(\pi^+\pi^-\pi^\circ)\pi^-]\pi^+$

Table 2
Masses and widths of the exotic states used in this study. The values are in MeV/c^2. The decay chains of the states are given as well. π° and η are always decaying into $\gamma\gamma$. Note that the decay of the $\omega(782) \to \pi\pi\pi$ cannot be simulated directly, but has to proceed via $\rho\pi$ (see Section 11 for details).

As an example the generated pion mass distributions for the reaction $\gamma p \to \eta_1(1800)p \to a_1^-(1260)\pi^+p \to [\rho^-\pi^\circ]\pi^+p \to [(\pi^\circ\pi^-)\pi^\circ]\pi^+p$ are shown in Figs 1. The three figures show the pion combinations that make up the intermediate resonances.

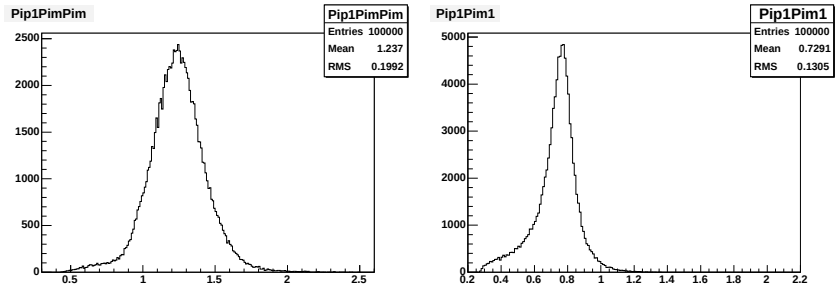

(a) $\pi^\circ\pi^-\pi^\circ$ (b) $\pi^\circ\pi^-$

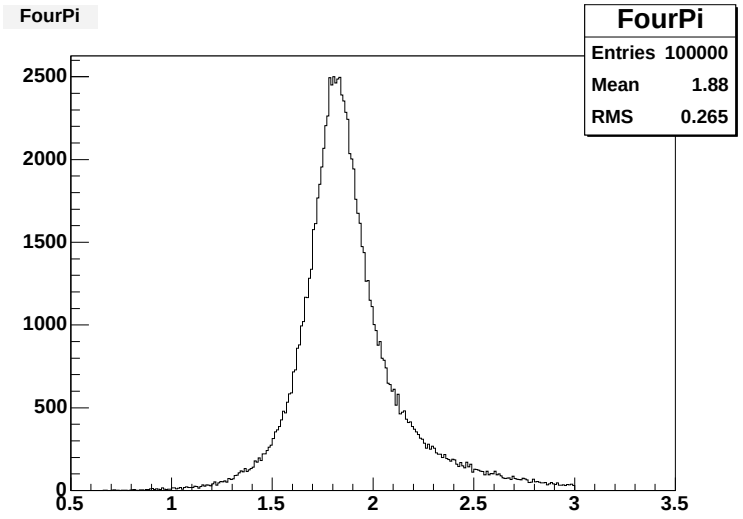

(c) $\pi^\circ\pi^-\pi^\circ\pi^+$

Fig. 1. Generated mass distributions for the resonances in Reaction 2 (see Table 2).

3 Particle losses

3.1 Charged Pions

Because of the peripheral production mechanism charged tracks in the events are mostly going forward. This is evident from Figs. 2(a) and 3(a), which show the distributions of the polar angle θ_π for the positive and negative pions from Reaction 1 (see Table 2), respectively. The acceptance for these events as a function of this angle is mostly flat, which can be seen in Figs. 2(b) and 3(b). The distributions were only plotted up to $\theta_\pi = 70^\circ$, because above this value the statistics for the events becomes too low for a comparison. Events going in the very forward direction ($\theta_\pi \approx 1^\circ$) are lost because the FDCs have a small hole in the middle in order to let non-interacting beam photons pass through.

This causes the drop in acceptance at very small angles, seen in Figs. 2(b) and 3(b).

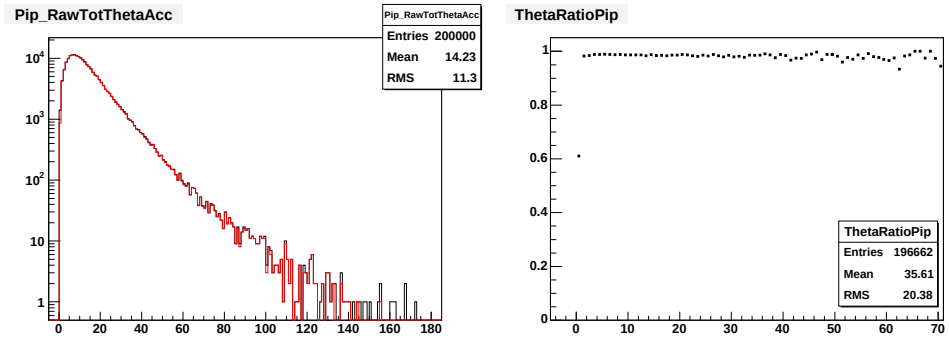

(a) (b)

Fig. 2. Acceptance as a function of the polar angle in the lab frame, $\theta_\pi^{\mathrm{Lab}}$ for all π^+ from Reaction 1 (see Table 2). (a) Number of events as a function of $\theta_\pi^{\mathrm{Lab}}$ (black: generated events, red: accepted events) (b) Acceptance as a function of $\theta_\pi^{\mathrm{Lab}}$.

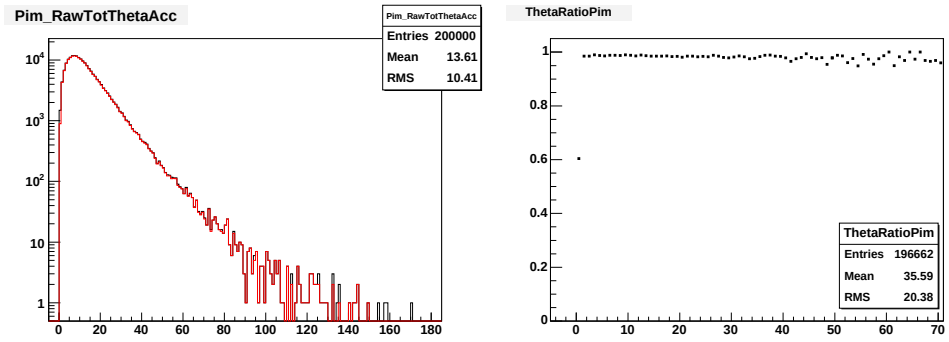

(a) (b)

Fig. 3. Acceptance as a function of the polar angle in the lab frame, $\theta_\pi^{\mathrm{Lab}}$ for all π^- from Reaction 1 (see Table 2). (a) Number of events as a function of $\theta_\pi^{\mathrm{Lab}}$ (black: generated events, red: accepted events) (b) Acceptance as a function of $\theta_\pi^{\mathrm{Lab}}$.

3.2 Photons

The acceptance for photons in the detector system is a more complicated because they cannot be tracked through the detector volume, but are observed from the deposited energy in a barrel calorimeter, BCAL, surrounding the target and a forward lead glass wall, LGD. Therefore they are lost if they do arrive at the BCAL or the LGD. Fig 4(a) shows the distribution of the laboratory angle $\theta_\gamma^{\mathrm{Lab}}$ for photons from the decay of neutral π and η from

Reaction 3 (see Table 2) for accepted events (red) as compared to the generated ones (black). The acceptance in Fig 4(b) shows that photons are lost at

- ◇ $\theta_\gamma^{\mathrm{Lab}} < 1°$.
  This loss is due to the beam hole in the LGD in order to let non-interacting beam particles pass through the detector.
- ◇ $\theta_\gamma^{\mathrm{Lab}} > 130°$.
  The coverage of the BCAL in the backward directions ends at approximately this angle.

A cartoon of the setup of the calorimetry for the experiment is given in appendix A.1. Values for the limiting angles for the acceptance in each detector are presented in appendix A.2, as well as a study for the size of the beam hole in the LGD.

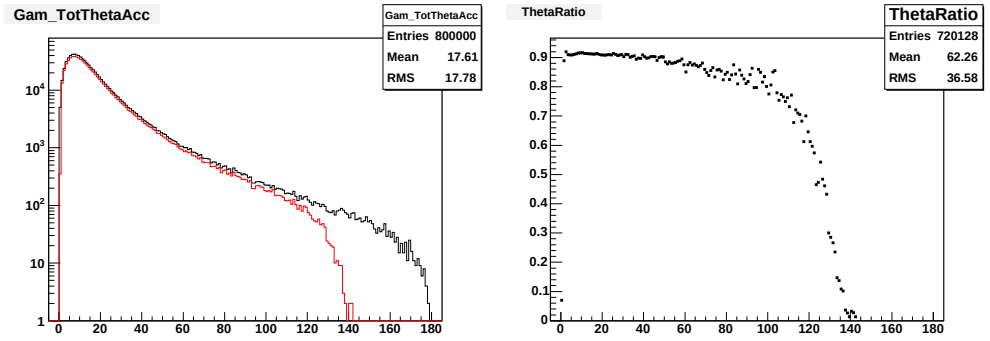

Fig. 4. Acceptance as a function of the polar angle in the lab frame, $\theta_\gamma^{\mathrm{Lab}}$ for all photons from Reaction 3 (see Table 2). (a) Number of events as a function of $\theta_\gamma^{\mathrm{Lab}}$ (black: generated events, red: accepted events) (b) Acceptance as a function of $\theta_\gamma^{\mathrm{Lab}}$.

4 Minimum energy deposition in BCAL and LGD

In order to reduce background noise in the BCAL and the LGD particles will have to deposit a minimum amount of energy in the detectors in order to be accepted for analysis. However, this will also reduce the number of accepted photons, since some of them will have low energies that may fall below these thresholds. Fig. 5 shows the low end of the energy spectrum for all photons, Figs. 6 and 7 the low energy spectrum if the corresponding photon is detected in the BCAL and the LGD, respectively. A minimum energy requirement of 20 MeV for photons detected in BCAL and of 100 MeV in the LGD reduces the number of accepted events for this reaction by about 10% and depends of course on the number of photons detected (see Fig. 8). The effect on the acceptance for each individual reaction will be given in the sections below.

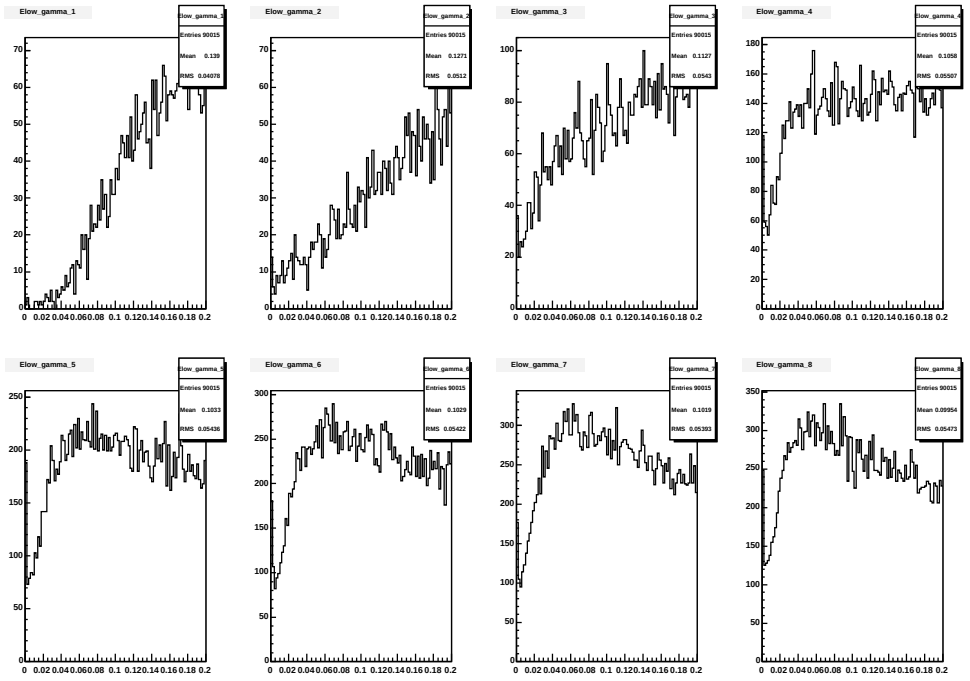

Fig. 5. E_γ for the 8 photons from Reaction 3 (see Table 2). Only the low end of the spectrum is shown.

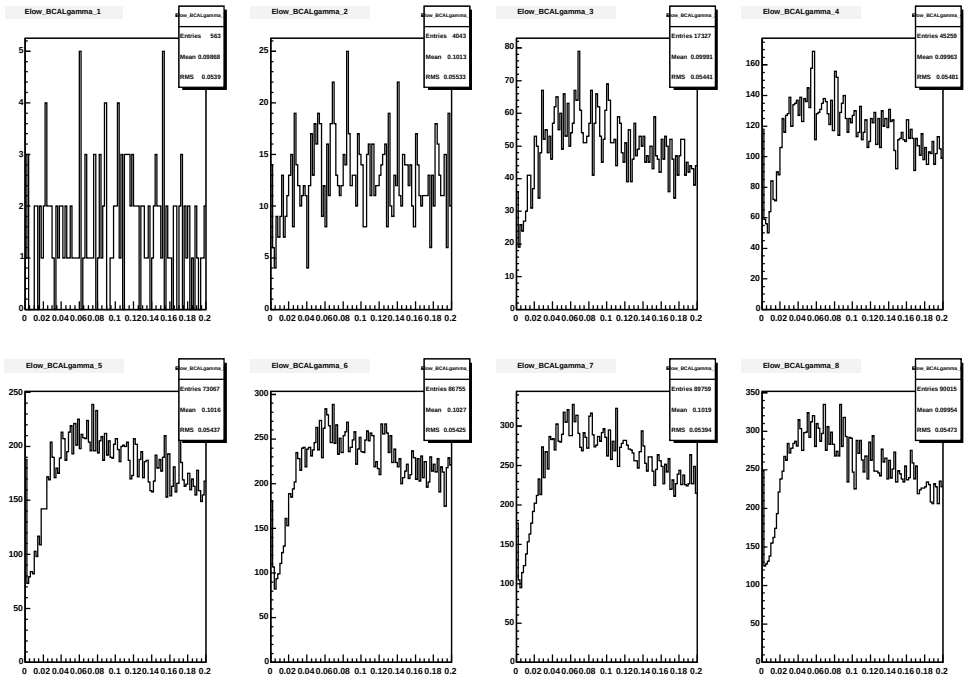

Fig. 6. E_γ for photons detected in BCAL for the 8 photons from Reaction 3 (see Table 2). Only the low end of the spectrum is shown.

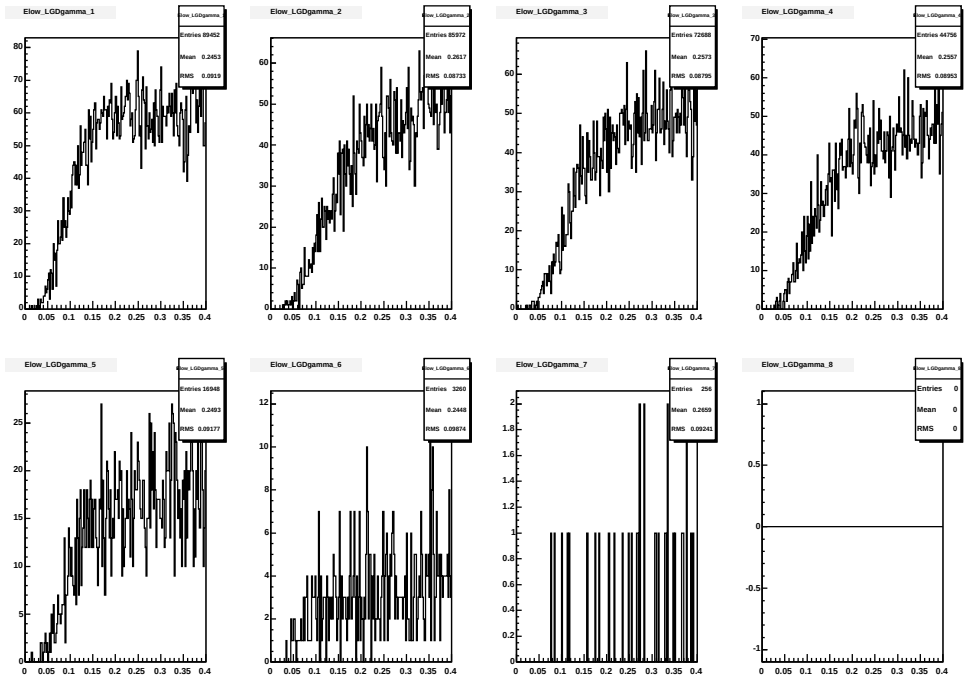

Fig. 7. E_γ for photons detected in LGD for the 8 photons from Reaction 3 (see Table 2). Only the low end of the spectrum is shown.

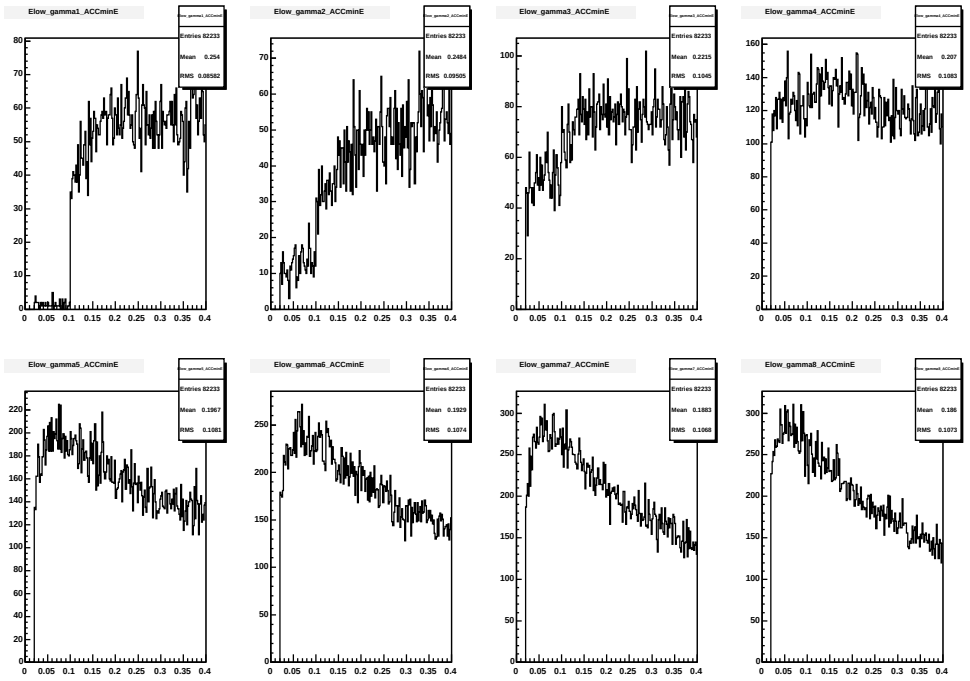

Fig. 8. E_γ for the 8 photons from Reaction 3 (see Table 2) after requiring minimum energy deposition in both the BCAL and the LGD. Only the low end of the spectrum is shown.

We also used the 8 photon final state of reaction 3 (see Table 2) to perform a study of the dependence of the acceptance on the minimum energy cutoffs. The results are listed in Table 3 and show that even with very strict cuts on the minimum energy the probability for a single photon to be accepted in the calorimeters never drops below 93%. For photon reconstruction it may therefore be possible to require even stricter minimum energy cuts than the 20 MeV and 100 MeV for BCAL and LGD photons, respectively, that were used for this study.

$BCAL\ [MeV]$	$LGD\ [MeV]$	*acc events* (A)	$A_\gamma = \sqrt[8]{A}$
20	100	82 233	97.58
30	100	77 441	96.86
40	100	72 375	96.04
50	100	67 238	95.16
60	100	62 065	94.21
70	100	57 181	93.25
20	110	81 725	97.51
20	120	81 156	97.42
20	130	80 517	97.33
20	140	79 841	97.23
20	150	79 064	97.11
20	160	78 279	96.99
20	170	77 473	96.86
40	120	71 397	95.88
40	140	70 205	95.68
60	120	61 180	94.04
60	140	60 125	93.84

Table 3
Total acceptance A and photon acceptance A_γ as a function of the minimum energy cutoffs in the BCAL and the LGD.

5 $\pi^\circ \to \gamma\gamma$ and $\eta \to \gamma\gamma$ selection

In order to reconstruct π° and η from $\gamma\gamma$ events one needs to perform cuts to select events that are compatible with decays from pions or etas. These

cuts usually will not only reduce background events, but throw out also some good events. We introduce a crude elliptical cut on the $\gamma\gamma$ mass for final states containing 4 photons. Higher multiplicities were not considered because the combinatorics would become too difficult to handle in a simple study like this one. For this topology the cut has the form

$$\begin{aligned} \frac{(m_{ij} - M_1)^2}{\Gamma_1^2} + \frac{(m_{kl} - M_2)^2}{\Gamma_2^2} &\leq 1 \\ \frac{(m_{kl} - M_1)^2}{\Gamma_1^2} + \frac{(m_{ij} - M_2)^2}{\Gamma_2^2} &\leq 1 \end{aligned} \tag{2}$$

where m_{ij} and m_{kl} are the three possible combinations of masses that one can make from the 4 photons [1], $M_{1,2}$ are the required masses (M_π or M_η) and $\Gamma_{1,2}$ are the semi axes of the ellipses, determining how wide the cut around the central mass should be. An event is accepted when any of the six possible conditions from Eq. 2 was fulfilled.

In Reaction 2 (see Table 2) we are looking for events containing $\pi^\circ\pi^\circ$, therefore $M_1 = M_2 = M_\pi = 135$ MeV and $\Gamma_1 = \Gamma_2 \equiv \Gamma$ was chosen to be $\Gamma = 65$ MeV.

Events from Reaction 4 (see Table 2) have a π° and an η in the final state, therefore the parameters for the cuts take slightly different values: $M_1 = M_\pi = 135$ MeV, $M_2 = M_\eta = 547$ MeV, $\Gamma_1 = 65$ MeV, and $\Gamma_2 = 85$ MeV.

Figs. 9 and 10 show the cut and the selected events for the above events and numbers on how the acceptance for photons will change due to this selection will be presented in the corresponding sections for these reactions.

[1] $\overline{(ij)(kl)} = (12)(34), (13)(24), (14)(23)$

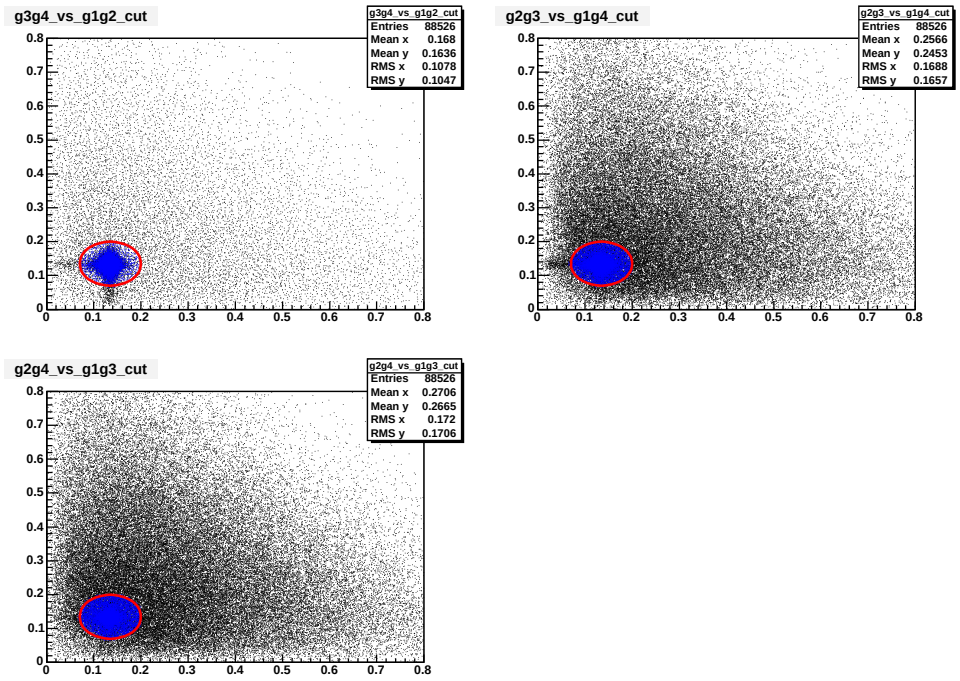

Fig. 9. $\gamma_k\gamma_l$ invariant mass vs $\gamma_i\gamma_j$ invariant mass for events from Reaction 2 (see Table 2). The colored area indicates events that are accepted by the elliptical cut in order to select the neutral meson topology $\pi^\circ\pi^\circ$.

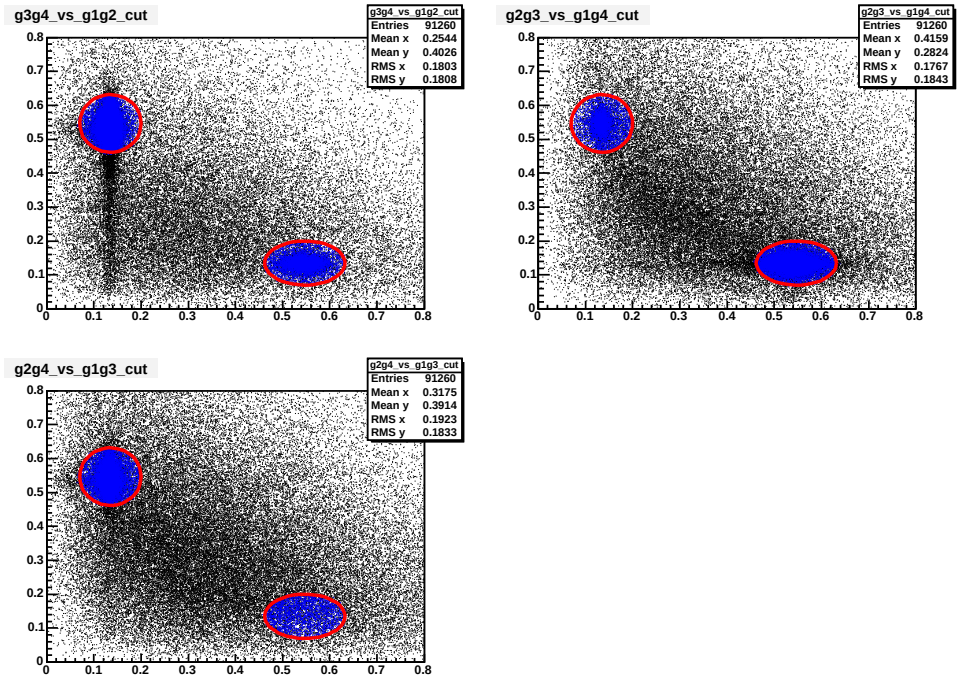

Fig. 10. $\gamma_k\gamma_l$ invariant mass vs $\gamma_i\gamma_j$ invariant mass for events from Reaction 4 (see Table 2). The colored area indicates events that are accepted by the elliptical cut in order to select the neutral meson topology $\pi^\circ\eta$.

6 Results for $\gamma p \to \eta_1(1800) p \to \pi^+\pi^-\pi^+\pi^- p$ (Reaction 1)

$$
\begin{aligned}
\gamma p &\to \eta_1 p \\
&\quad \eta_1 \to a_1^- \pi^+ \\
&\quad\quad a_1^- \to \rho^\circ \pi^- \\
&\quad\quad\quad \rho^\circ \to \pi^+ \pi^-
\end{aligned}
$$

6.1 Accepted events totals

For Reaction 1 (see Table 2) 98 331 events were accepted after the running the 100 000 generated events through the detector geometry in `HDFast`. Since this reaction has only charged particles in the final state the acceptance for a charged pion in the detector is given by [2]

$$
\begin{aligned}
A_{\mathrm{c}}^4 &= 0.98331 \\
\Rightarrow A_{\mathrm{c}} &= \sqrt[4]{0.98331} \\
&= 0.9958
\end{aligned}
$$

This number will be used in other reactions that involve both charged particles and photons in the final state. An overview over the numbers is given in Table 4.

	# of events	A_{tot}	A_{c}	A_γ
Gen	100 000	100 %	100 %	N/A
Geo	98 331	98.33 %	99.58 %	N/A
minE	N/A			
γSel	N/A			

Table 4
Event totals and acceptance for Reaction 1 (see Table 2). Gen = generated events, Geo = after geometrical acceptance, minE = after minimum energy cut on photons detected in LGD and BCAL, γSel = elliptical cut on $\gamma\gamma$ masses.

6.2 Acceptance as a function of M_{tot}

Fig. 11(b) shows a plot of the acceptance as function of total meson mass M_{tot}, which is obtained from the distributions in Fig. 11(a): $A = N_{\mathrm{acc}}/N_{\mathrm{gen}}$. As can be seen the acceptance is flat over the range of the distribution where

[2] We assume that the acceptance is equal for positive and negative pions.

the $\eta_1(1800)$ is peaking. The variations below $M_{\mathrm{tot}} = 1.5$ GeV/c^2 and above $M_{\mathrm{tot}} = 2.5$ GeV/c^2 are due to a lack of statistics in those regions.

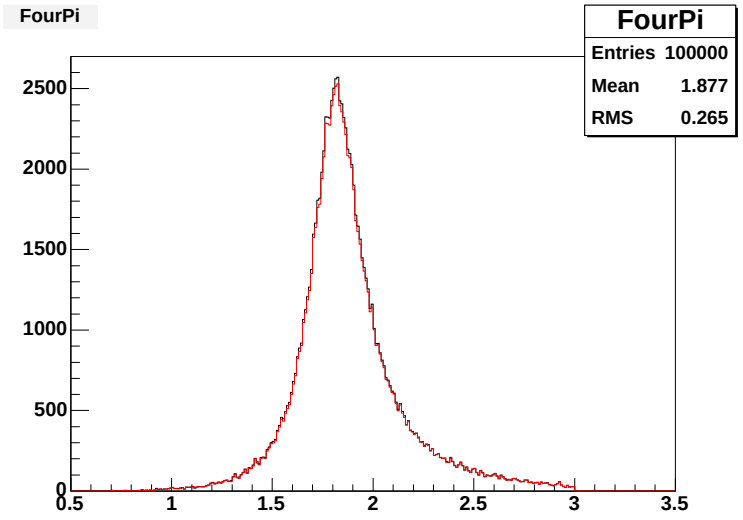

(a) M_{tot}. Black: generated, red: accepted events

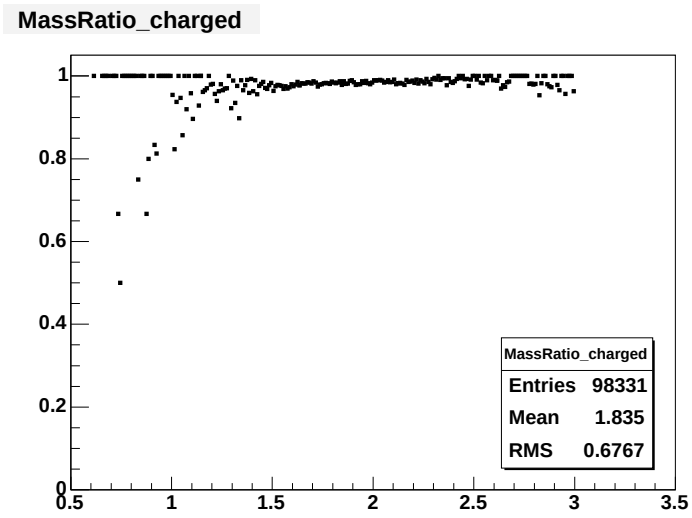

(b) Acceptance

Fig. 11. Acceptance as a function of M_{tot} for Reaction 1 (see Table 2).

6.3 Acceptance as a function of helicity angles

We also determined the acceptance as a function of the various angles used in the PWA. For Reaction 1 there are three sets of angles:

- ◇ Gottfried-Jackson frame: θ_{GJ} and ϕ_{TY}
  The Gottfried-Jackson frame is the restframe of the produced resonance (here $\eta_1(1800)$), aligned so that $\hat{z}_{GJ}$ is in direction of the beam, $\hat{y}_{GJ}$ is perpendicular to the production plane, and $\hat{x}_{GJ} = \hat{y}_{GJ} \times \hat{z}_{GJ}$
- ◇ Helicity frame of Isobar 1: θ_1^h and ϕ_1^h
  This is the restframe of the first isobar (here $a_1^-(1260)$). Again the frame is aligned in a unique manner: $\hat{z}_{h1}$ is in direction of the a_1 before the boost into its restframe, $\hat{y}_{h1}$ is perpendicular to both $\hat{z}_{GJ}$ and $\hat{z}_1^h$, and $\hat{x}_1^h = \hat{y}_1^h \times \hat{z}_1^h$
- ◇ Helicity frame of Isobar 2: θ_2^h and ϕ_2^h
  This is the restframe of the second isobar (here $\rho^\circ(770)$). The frame is aligned analogous to the Helicity frame of Isobar 1.

Fig. 14 shows the acceptance as a function of these 6 angles.

In all cases the distributions are flat and close to unity, with the exception of $\cos(\theta_{GJ}) = \pm 1$. Since the z-axis in the Gottfried-Jackson frame is defined by the direction of the beam (same as the z-axis in the lab frame), the π^+ from the decay of the $\eta_1(1800)$ (the recoil to the $a_1^-(1260)$) will mostly be emitted in the forward direction for events where $|\cos(\theta_{GJ})| \lesssim 1.0$. Because of the beam hole in the forward drift chambers this π^+ has a high probability to escape detection and the event will be lost. This is demonstrated in Fig. 12, which shows the distribution of θ_π^{Lab} for the recoil π^+ for events with $0.9 \leq |\cos(\theta_{GJ})| \leq 1.0$.

The slight drop in the acceptance at $\phi_{TY} = 0$ is very likely caused by the same effect, because the ϕ angle is poorly determined for a particle with $\theta = 0$. Fig. 13(a) shows that there is an enhancement at $\theta_\pi^{\text{Lab}} = 0$ for the recoil π^+ from the $\eta_1(1800)$ decay if one selects events in the vicinity of $\phi_{TY} = 0$ as compared to the other π in the reaction.

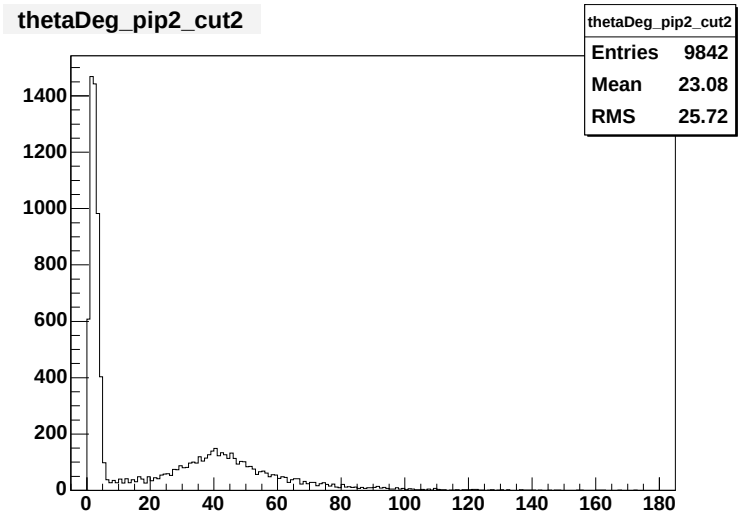

Fig. 12. $\theta_{\pi}^{\mathrm{Lab}}$ for the recoil π^{+} to the a_1^{-} for events with $0.9 \leq |\cos(\theta_{GJ})| \leq 1.0$.

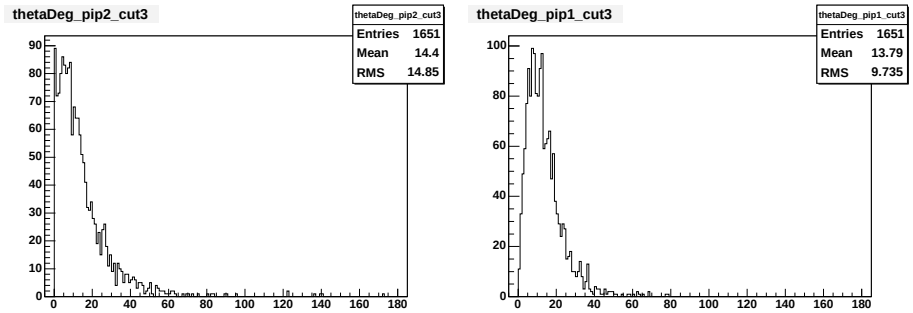

(a) π_1^{+} (b) π_2^{+}

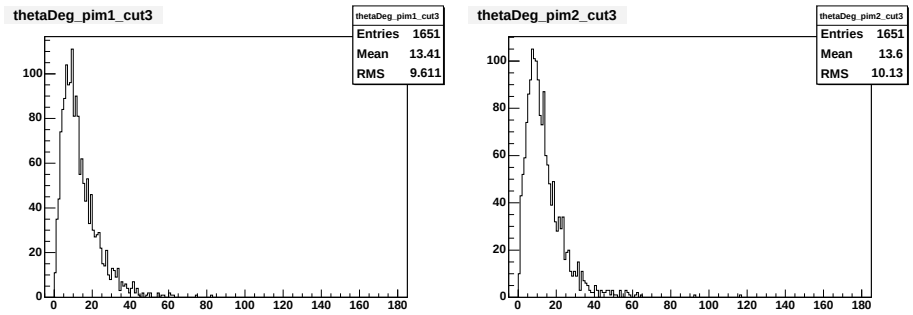

(c) π_1^{-} (d) π_2^{-}

Fig. 13. $\theta_{\pi}^{\mathrm{Lab}}$ for events with $|\phi_{TY}| \leq 0.05$ rad from Reaction 1 (see Table 2).

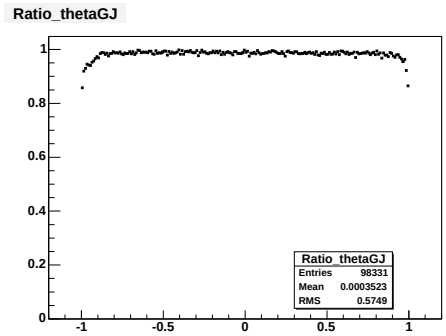

(a) $\cos(\theta_{GJ})$

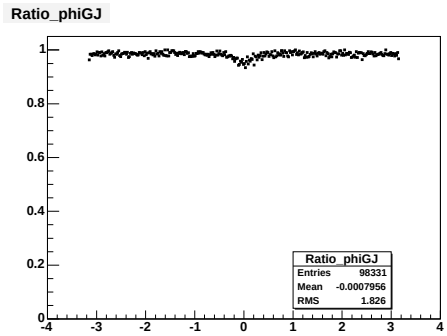

(b) ϕ_{TY}

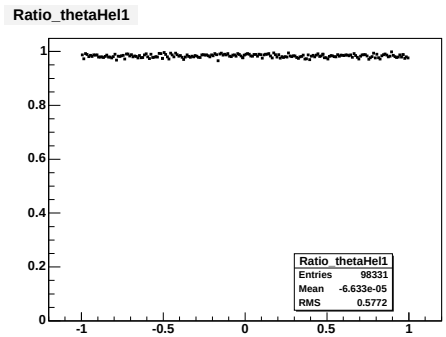

(c) $\cos(\theta_1^h)$

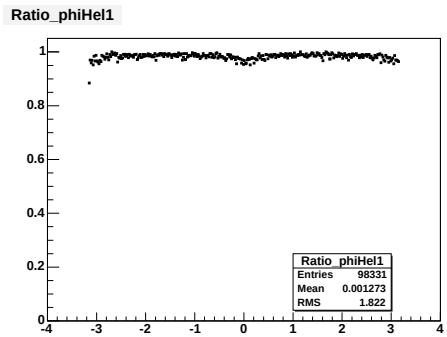

(d) ϕ_1^h

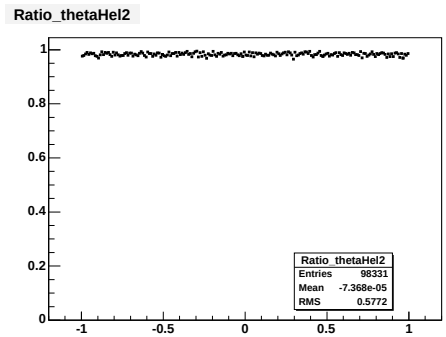

(e) $\cos(\theta_2^h)$

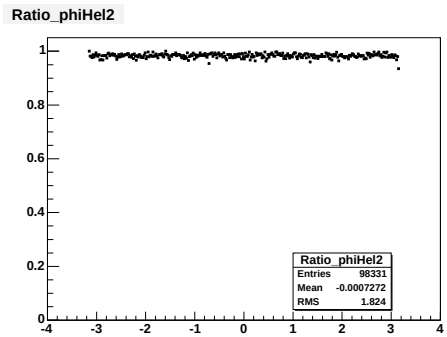

(f) ϕ_2^h

Fig. 14. Acceptance as a function of the various angles used in the PWA for Reaction 1 (see Table 2).

7 Results for $\gamma p \to \eta_1(1800) p \to \pi^+\pi^- 4\gamma\ p$ (Reaction 2)

$$
\begin{aligned}
\gamma p &\to \eta_1 p \\
&\quad \eta_1 \to a_1^- \pi^+ \\
&\qquad a_1^- \to \rho^- \pi^\circ \ , \quad \pi^\circ \to \gamma\gamma \\
&\qquad\quad \rho^- \to \pi^- \pi^\circ \, , \quad \pi^\circ \to \gamma\gamma
\end{aligned}
$$

7.1 Accepted events totals

For Reaction 2 (see Table 2) 93 712 events survived running the generated events through the geometry of the detector system. This results in an acceptance for single photons, A_γ, of

$$
\begin{aligned}
A_{\text{tot}} &= A_{\text{c}}^2 \cdot A_\gamma^4 \\
&= 0.93712 \\
\Rightarrow A_\gamma &= \sqrt[4]{\frac{0.93712}{A_{\text{c}}^2}} \\
&= 0.9860
\end{aligned}
$$

where we have used $A_{\text{c}} = 99.58$ % (see Table 4). With the minimum energy cut in the BCAL and the LGD the data set shrinks to 88 526 events and, lastly, performing the elliptical cut reduces the set to 86 853 events. Table 5 gives an overview over all the data sets and the calculated photon acceptance.

	# of events	A_{tot}	A_{c}	A_γ
Gen	100 000	100 %	100 %	100 %
Geo	93 712	93.71 %	99.58 %	98.60 %
minE	88 526	88.53 %	99.58 %	97.20 %
γSel	86 853	86.85 %	99.58 %	96.74 %

Table 5
Event totals and acceptance for Reaction 2 (see Table 2). Gen = generated events, Geo = after geometrical acceptance, minE = after minimum energy cut on photons detected in LGD and BCAL, γSel = elliptical cut on $\gamma\gamma$ masses.

7.2 Acceptance as a function of M_{tot}

Again, the acceptance as a function of total meson mass M_{tot} shows a flat, structureless behavior over the peak of the $\eta_1(1800)$ resonance (see Fig. 15). The variations at lower and higher 4π mass are due to statistical fluctuations.

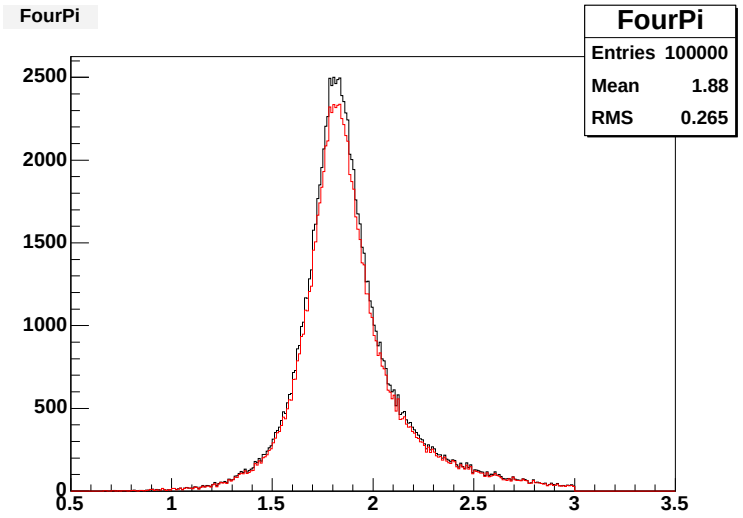

(a) M_{tot}. Black: generated, red: accepted events

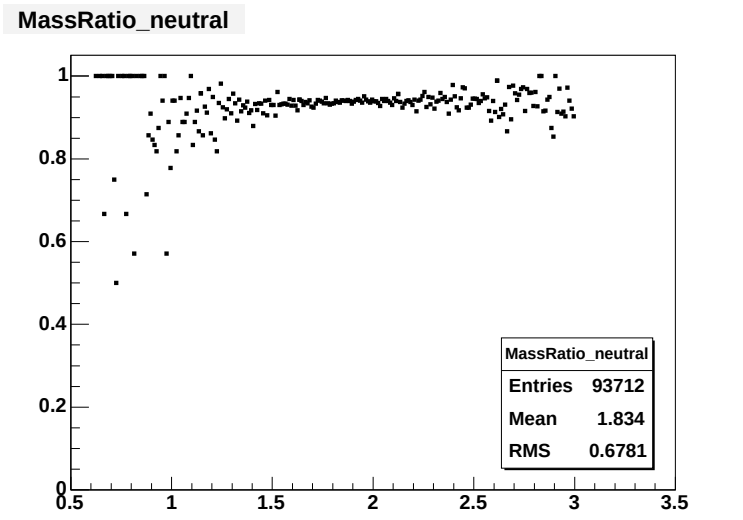

(b) Acceptance

Fig. 15. Acceptance as a function of M_{tot} for Reaction 2 (see Table 2).

7.3 Acceptance as a function of helicity angles

Fig. 16 shows the acceptance as a function of the angles used in the PWA for this reaction. The distributions again show no evident structure, with the exception of the drop at $|\cos(\theta_{GJ})| \approx 1$ and at $\phi_{TY} \approx 0$ deg, which were already explained in section 6.3.

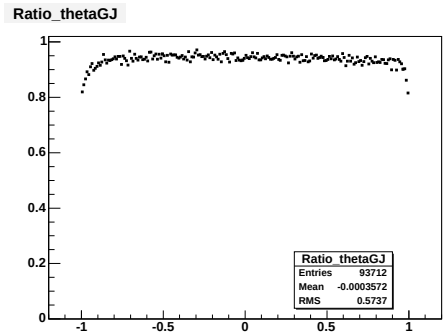

(a) $\cos(\theta_{GJ})$

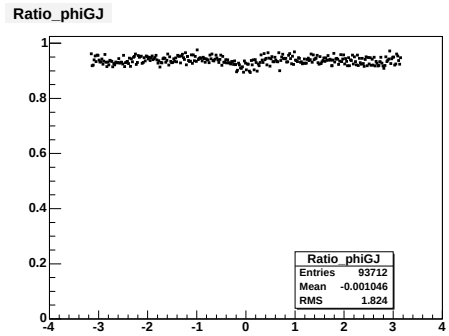

(b) ϕ_{TY}

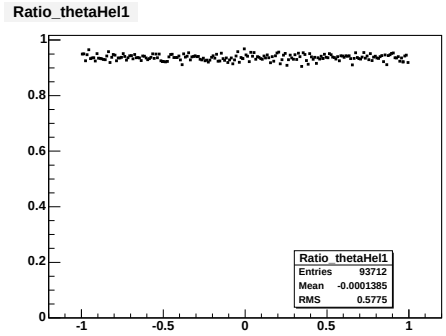

(c) $\cos(\theta_1^h)$

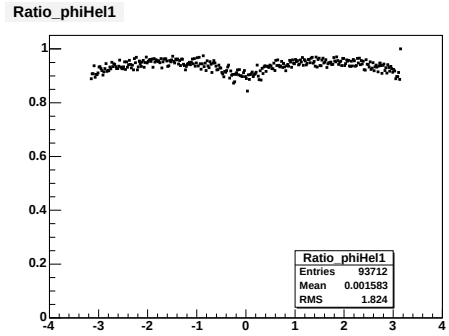

(d) ϕ_1^h

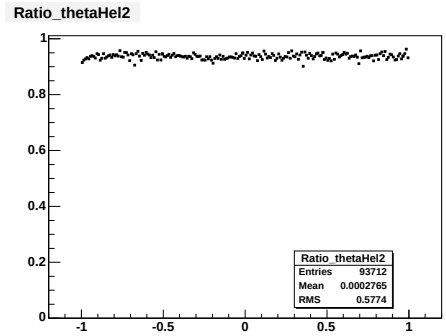

(e) $\cos(\theta_2^h)$

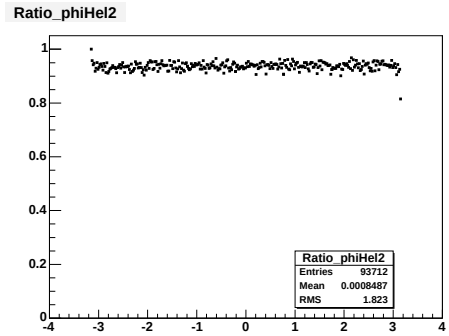

(f) ϕ_2^h

Fig. 16. Acceptance as a function of the various angles used in the PWA for Reaction 2 (see Table 2).

8 Results for $\gamma p \to \pi_1^\circ(1700) p \to 8\gamma\ p$ (Reaction 3)

$$
\begin{aligned}
\gamma p \to \pi_1^\circ p & \\
\pi_1^\circ \to f_1 \pi^\circ\ , \ \pi^\circ \to \gamma\gamma & \\
f_1 \to a_0^\circ \pi^\circ \quad , \quad \pi^\circ \to \gamma\gamma & \\
a_0^\circ \to \pi^\circ \eta \quad , \quad \pi^\circ, \eta \to \gamma\gamma &
\end{aligned}
$$

8.1 Accepted events totals

Reaction 3 is very interesting, because the final state contains only photons and no charged particles. 90 016 events were accepted after running `HDFast`. This leads to a single-photon acceptance, A_γ, of

$$
\begin{aligned}
A_{\text{tot}} &= A_\gamma^8 \\
&= 0.90016 \\
\Rightarrow A_\gamma &= \sqrt[8]{0.90016} \\
&= 0.9869
\end{aligned}
$$

The additional constraint for the minimum energy deposited in the BCAL and the LGD reduces the date set to 82 234 events. Table 6 gives an overview over all the data sets and the calculated photon acceptances.

	# of events	A_{tot}	A_{c}	A_γ
Gen	100 000	100 %	N/A	100 %
Geo	90 016	90.02 %	N/A	98.69 %
minE	82 234	82.23 %	N/A	97.59 %
γSel	N/A			

Table 6
Event totals and acceptance for Reaction 3 (see Table 2). Gen = generated events, Geo = after geometrical acceptance, minE = after minimum energy cut on photons detected in LGD and BCAL, γSel = elliptical cut on $\gamma\gamma$ masses.

8.2 Acceptance as a function of M_{tot}

The acceptance as a function of the total meson mass M_{tot}, shown in Fig. 17(b), is again structureless and flat over the peak of the generated $\pi_1(1700)$. The

larger fluctuations in the regions below 1.5 GeV/c^2 and above 2.5 GeV/c^2 are again caused by lack of statistics.

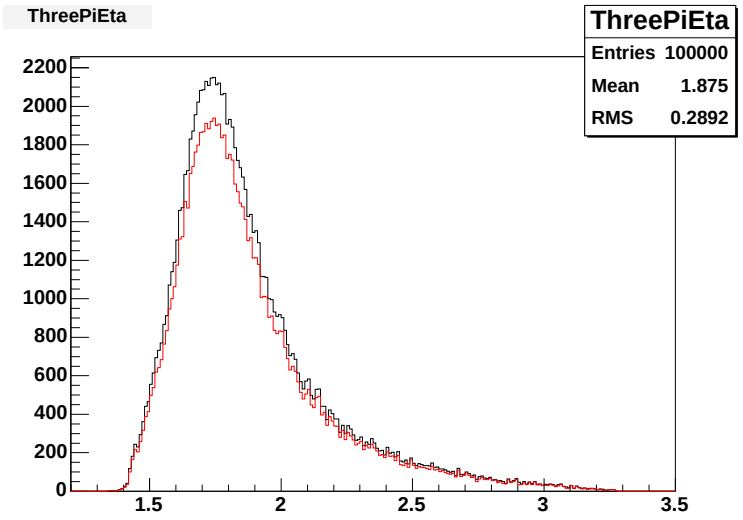

(a) M_{tot}. Black: generated, red: accepted events

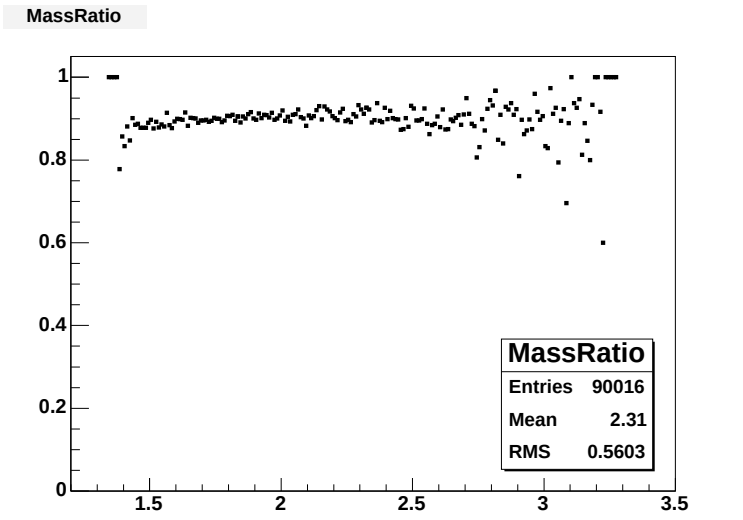

(b) Acceptance

Fig. 17. Acceptance as a function of M_{tot} for Reaction 3 (see Table 2).

8.3 Acceptance as a function of helicity angles

Fig. 18 shows the acceptance as a function of the angles used in the PWA for this reaction. With the exception of the drop at $|\cos(\theta_{GJ})| \approx 1$ all of the distributions are flat over the whole range for each of the angles and none shows any structure. It is interesting to note that the effect of missing the recoil particle into the beam hole also holds for a neutral meson decaying into two photons. In section 6.3 the effect was only demonstrated for a charged particle recoiling against the primary isobar. We will show this later in detail in section 10.3.

Reconstruction of this all neutral final state will be a very difficult task because of the many possible combinations to form 4 neutral mesons from 8 photons and was not attempted for this study. For the present final state this reconstruction will very likely be the dominating effect on the acceptance and might cause some structure as a function of the helicity angles.

For the all neutral final state we have also performed a study of the acceptance with an imperfect (non-hermetic) calorimetry system. The results of the study are shown in appendix B.

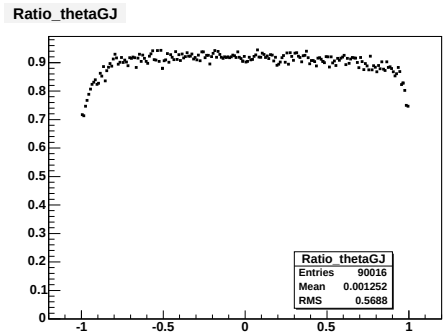

(a) $\cos(\theta_{GJ})$

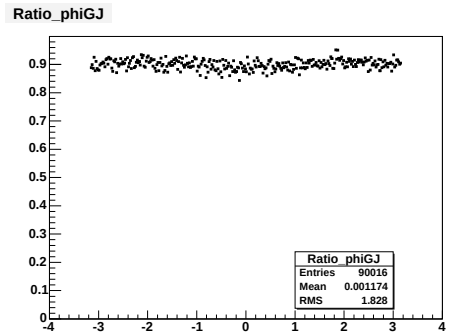

(b) ϕ_{TY}

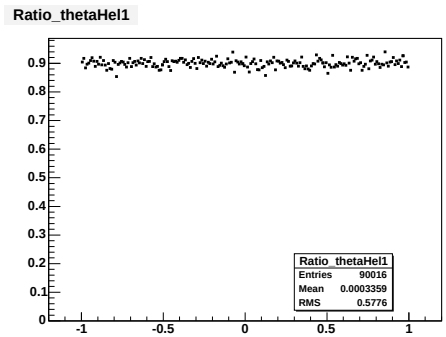

(c) $\cos(\theta_1^h)$

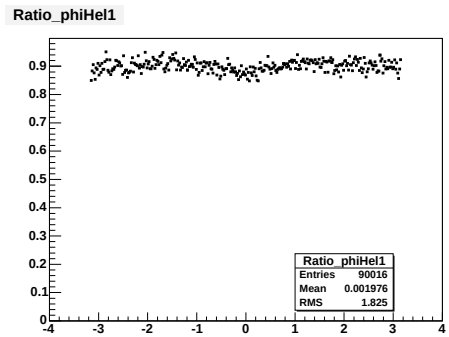

(d) ϕ_1^h

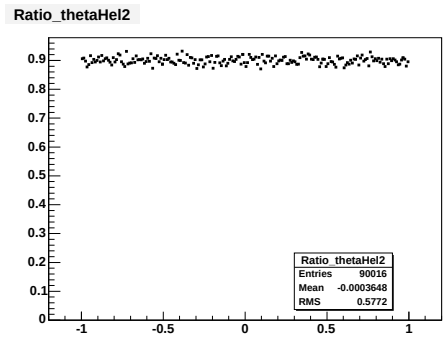

(e) $\cos(\theta_2^h)$

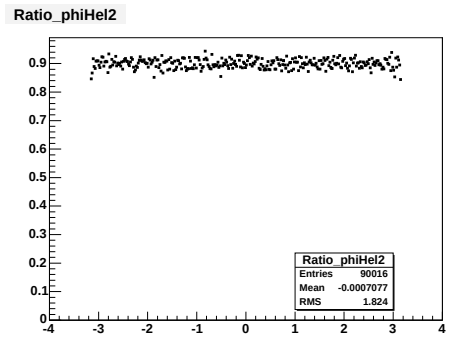

(f) ϕ_2^h

Fig. 18. Acceptance as a function of the various angles used in the PWA for Reaction 3 (see Table 2).

9 Results for $\gamma p \to \pi_1^\circ(1700) p \to \pi^+\pi^- 4\gamma\ p$ (Reaction 4)

$$
\begin{aligned}
\gamma p \to\ & \pi_1^\circ p \\
& \pi_1^\circ \to a_1^\circ \eta \ \ , \ \eta \to \gamma\gamma \\
& \quad a_1^\circ \to \rho^+\pi^- \\
& \quad\quad \rho^+ \to \pi^+\pi^\circ\,, \quad \pi^\circ \to \gamma\gamma
\end{aligned}
$$

9.1 Accepted events totals

For Reaction 4 (see Table 2) 94 514 events survived running the generated events through the geometry of the detector system. This results in an acceptance for single photons, A_γ, of

$$
\begin{aligned}
A_{\text{tot}} &= A_{\text{c}}^2 \cdot A_\gamma^4 \\
&= 0.94514 \\
\Rightarrow A_\gamma &= \sqrt[4]{\frac{0.94514}{A_{\text{c}}^2}} \\
&= 0.9881
\end{aligned}
$$

where we have used $A_{\text{c}} = 99.58$ % (see Table 4). With the minimum energy cut in the BCAL and the LGD the data set shrinks to 91 260 events and, lastly, performing the elliptical cut reduces the set to 86 180 events. Table 7 gives an overview over all the data sets and the calculated photon acceptance.

	# of events	A_{tot}	A_{c}	A_γ
Gen	100 000	100 %	100 %	100 %
Geo	94 514	94.51 %	99.58 %	98.81 %
minE	91 260	91.26 %	99.58 %	97.95 %
γSel	86 180	86.18 %	99.58 %	96.55 %

Table 7
Event totals and acceptance for Reaction 4 (see Table 2). Gen = generated events, Geo = after geometrical acceptance, minE = after minimum energy cut on photons detected in LGD and BCAL, γSel = elliptical cut on $\gamma\gamma$ masses.

9.2 Acceptance as a function of M_{tot}

The acceptance as a function of the total meson mass, M_{tot}, is again structureless and flat over the peak of the $\pi_1(1700)$. Again, the variations below $M_{\mathrm{tot}} = 1.5$ GeV/c^2 and above $M_{\mathrm{tot}} = 2.5$ GeV/c^2 are caused by a lack of statistics in these regions.

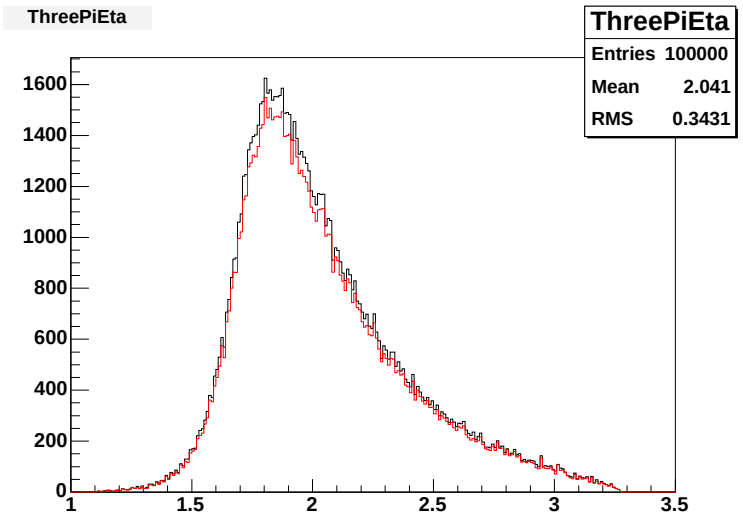

(a) M_{tot}. Black: generated, red: accepted events

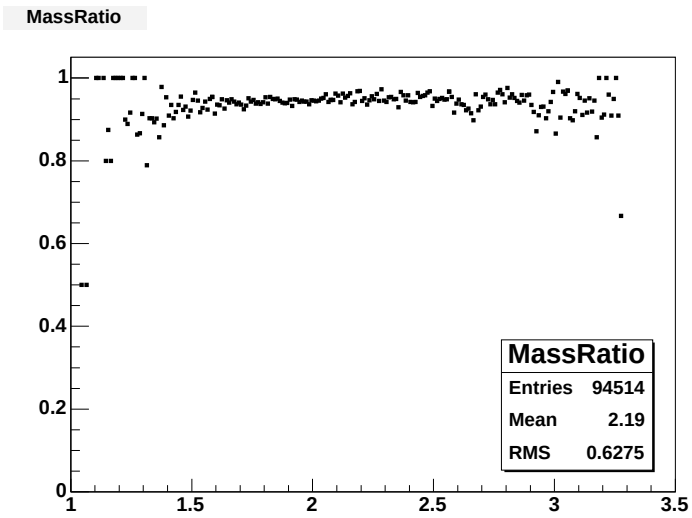

(b) Acceptance

Fig. 19. Acceptance as a function of M_{tot} for Reaction 4 (see Table 2).

9.3 Acceptance as a function of helicity angles

Fig. 20 shows the acceptance as a function of the angles used in the PWA for this reaction. Again, with the exception of the acceptance as a function of $\cos(\theta_{GJ})$, all of the distributions are flat over the whole range for each of the angles and none shows any evident structure. The drop at $|\cos(\theta_{GJ})| \approx 1$ is again due to the recoil meson to the primary isobar escaping detection. The effect is not as strong as before because the η is heavier than a π and can therefore carry more momentum perpendicular to the beam axis, which makes it less likely that a photon from the decay $\eta \to \gamma\gamma$ is missed in the beam hole of the LGD.

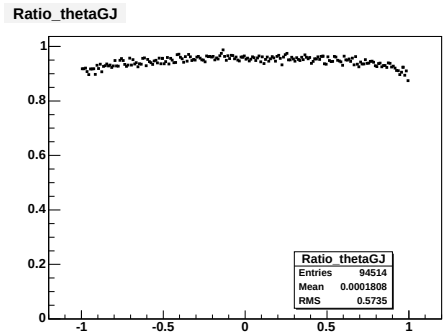

(a) $\cos(\theta_{GJ})$

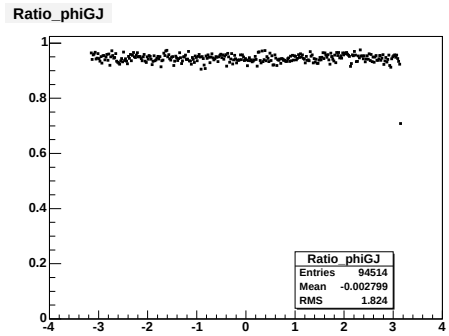

(b) ϕ_{TY}

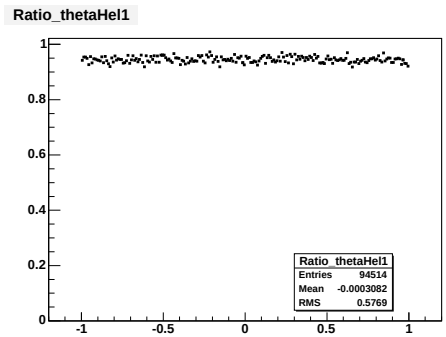

(c) $\cos(\theta_1^h)$

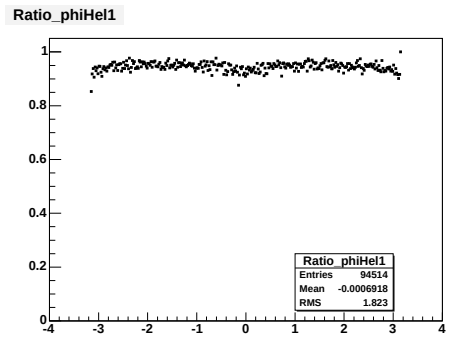

(d) ϕ_1^h

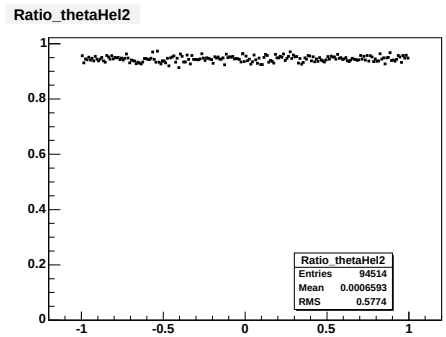

(e) $\cos(\theta_2^h)$

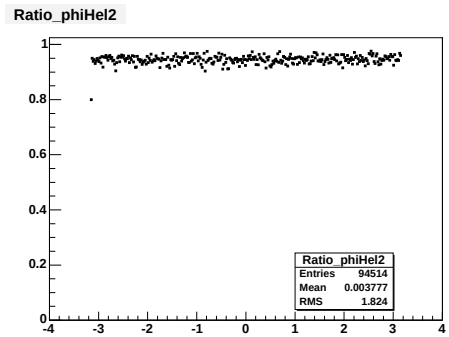

(f) ϕ_2^h

Fig. 20. Acceptance as a function of the various angles used in the PWA for Reaction 4 (see Table 2).

10 Results for $\gamma p \to b_2^+(2000) n \to \pi^+ 6\gamma\ n$ (Reaction 5)

$$
\begin{aligned}
\gamma p \to\ & b_2^+ n \\
& b_2^+ \to a_1^+ \pi^\circ,\ \pi^\circ \to \gamma\gamma \\
& \quad a_1^+ \to \rho^+ \pi^\circ\ ,\quad \pi^\circ \to \gamma\gamma \\
& \quad\ \rho^+ \to \pi^+ \pi^\circ\ ,\quad \pi^\circ \to \gamma\gamma
\end{aligned}
$$

10.1 Accepted events totals

For Reaction 5 (see Table 2) 91 914 events survived running the generated events through the geometry of the detector system. This results in an acceptance for single photons, A_γ, of

$$
\begin{aligned}
A_{\mathrm{tot}} &= A_{\mathrm{c}} \cdot A_\gamma^6 \\
&= 0.91914 \\
\Rightarrow A_\gamma &= \sqrt[6]{\frac{0.91914}{A_{\mathrm{c}}}} \\
&= 0.9867
\end{aligned}
$$

where we have used $A_{\mathrm{c}} = 99.58\ \%$ (see Table 4). With the minimum energy cut in the BCAL and the LGD the data set shrinks to 84 284 events. The elliptical cut was not performed in this case, because of the many possible combinations to make 3 neutral pions from 6 photons. Table 8 gives an overview over all the data sets and the calculated photon acceptance.

	# of events	A_{tot}	A_{c}	A_γ
Gen	100 000	100 %	100 %	100 %
Geo	91 914	91.91 %	99.58 %	98.67 %
minE	84 284	84.28 %	99.58 %	97.26 %
γSel	N/A			

Table 8
Event totals and acceptance for Reaction 5 (see Table 2). Gen = generated events, Geo = after geometrical acceptance, minE = after minimum energy cut on photons detected in LGD and BCAL, γSel = elliptical cut on $\gamma\gamma$ masses.

10.2 Acceptance as a function of M_{tot}

The acceptance as a function of the total meson mass, M_{tot}, again shows a flat, structureless behavior over the peak of the generated $b_2(2000)$ resonance (see Fig. 21). The fluctuations in the regions below 1.6 GeV/c^2 and above 2.6 GeV/c^2 are again caused by lack of statistics in these regions.

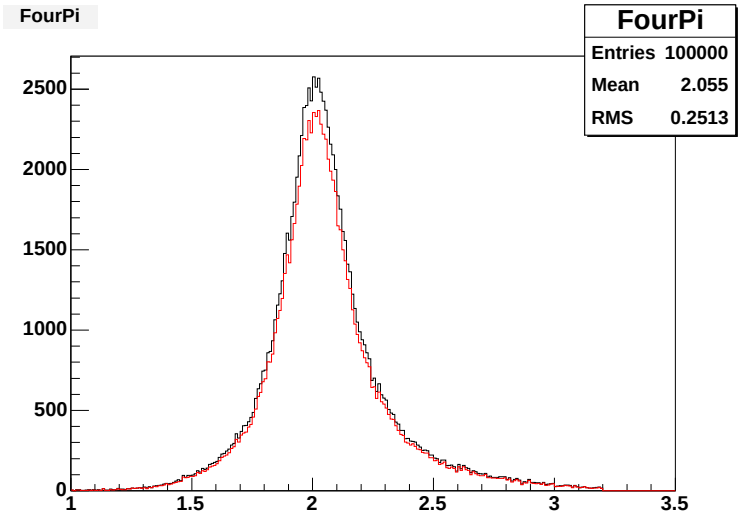

(a) M_{tot}. Black: generated, red: accepted events

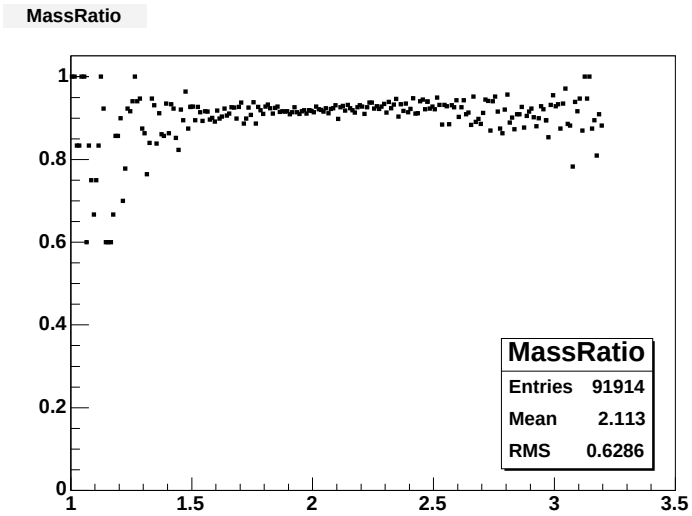

(b) Acceptance

Fig. 21. Acceptance as a function of M_{tot} for Reaction 5 (see Table 2).

10.3 Acceptance as a function of helicity angles

Fig. 23 shows the acceptance as a function of the angles used in the PWA for this reaction. Except for the $\cos(\theta_{GJ})$ and the ϕ_{TY} distributions the curves again show no evident structure. In this reaction the recoil to the first isobar (a_1^+) is a π° decaying into $\gamma\gamma$. It is interesting to note that the effect seen in section 6.3 with a charged π as the recoil to the primary isobar also holds here for a neutral meson. Fig. 22 shows that the photons from the decay of the π° recoil also are emitted preferably into the forward direction and can escape detection when they miss the LGD through the 4×4 block beam hole (see Appendix A).

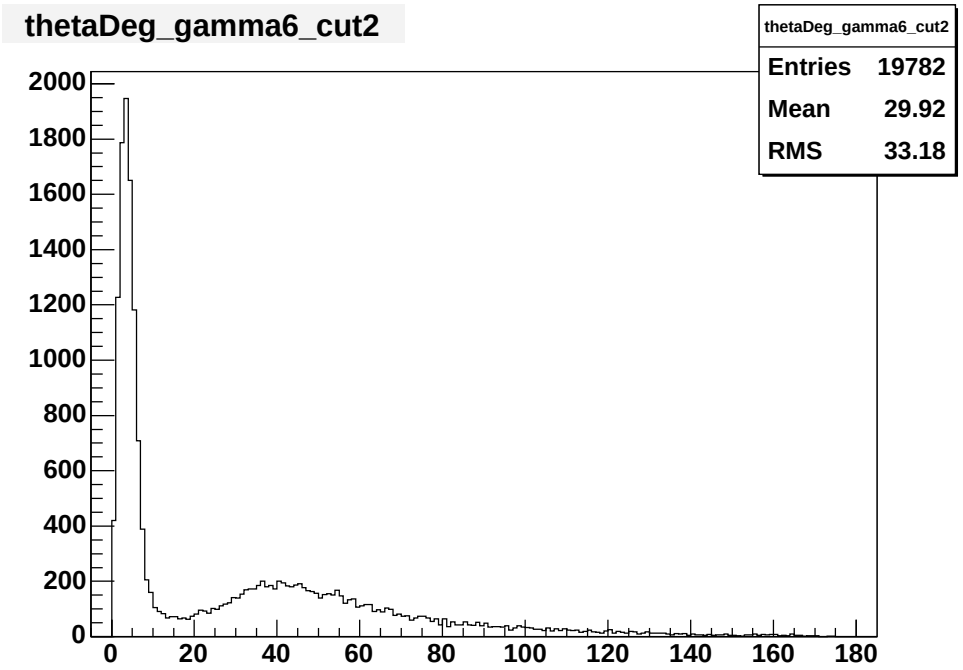

Fig. 22. $\theta_\gamma^{\mathrm{Lab}}$ for one of the two photons from the decay of the recoil π° to the a_1^+ for events with $0.8 \leq |\cos(\theta_{GJ})| \leq 1.0$.

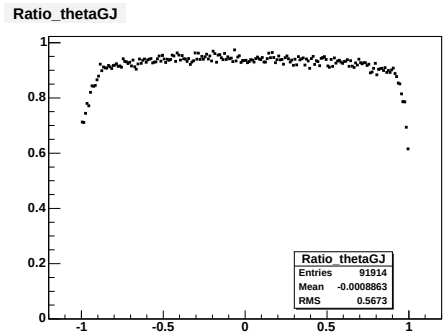

(a) $\cos(\theta_{GJ})$

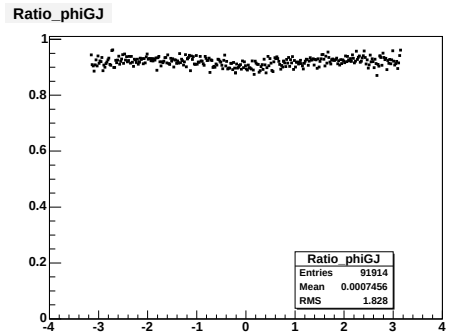

(b) ϕ_{TY}

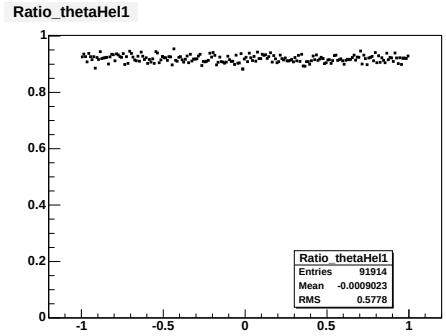

(c) $\cos(\theta_1^h)$

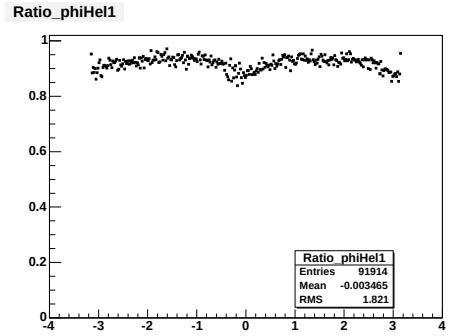

(d) ϕ_1^h

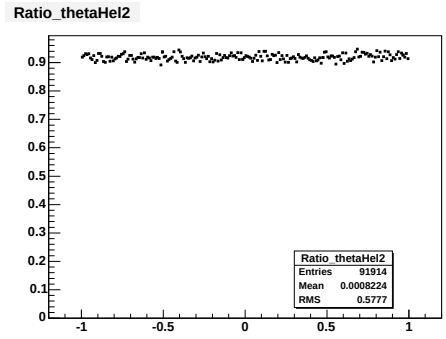

(e) $\cos(\theta_2^h)$

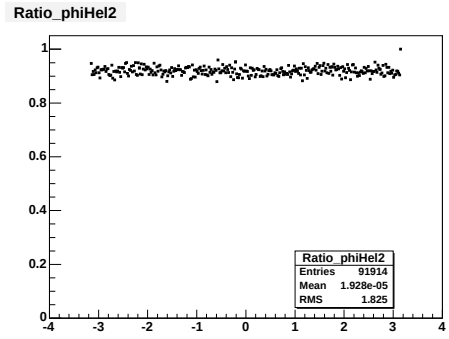

(f) ϕ_2^h

Fig. 23. Acceptance as a function of the various angles used in the PWA for Reaction 5 (see Table 2).

11 Results for $\gamma p \to \pi_1^+(1700) n \to \pi^+\pi^+\pi^- 4\gamma\ n$ (Reaction 6)

$$
\begin{aligned}
\gamma p \to \pi_1^+ n & \\
\pi_1^+ \to b_1^+ \pi^\circ\ , \ \pi^\circ \to \gamma\gamma & \\
b_1^+ \to \omega\pi^+ & \\
\omega \to \pi^+\pi^-\pi^\circ\ , \quad \pi^\circ \to \gamma\gamma &
\end{aligned}
$$

11.1 Accepted events totals

In this reaction the final state contains an ω, decaying into three pions. Since `genr8` cannot generate direct three-particle decays the final state was populated assuming that the decay proceeds via an intermediate ρ

$$\omega \to \rho\pi \to \pi\pi\pi$$

This reaction is possible even though the mass of the omega is lower than the sum of the masses of the ρ and a π, because the width of the ρ is rather large ($\Gamma = 150$ MeV/c^2). Fig. 24 shows the $\pi\pi$ mass of the two pions from the ρ decay. Note, that the ρ is not considered as an isobar in this reaction, but only

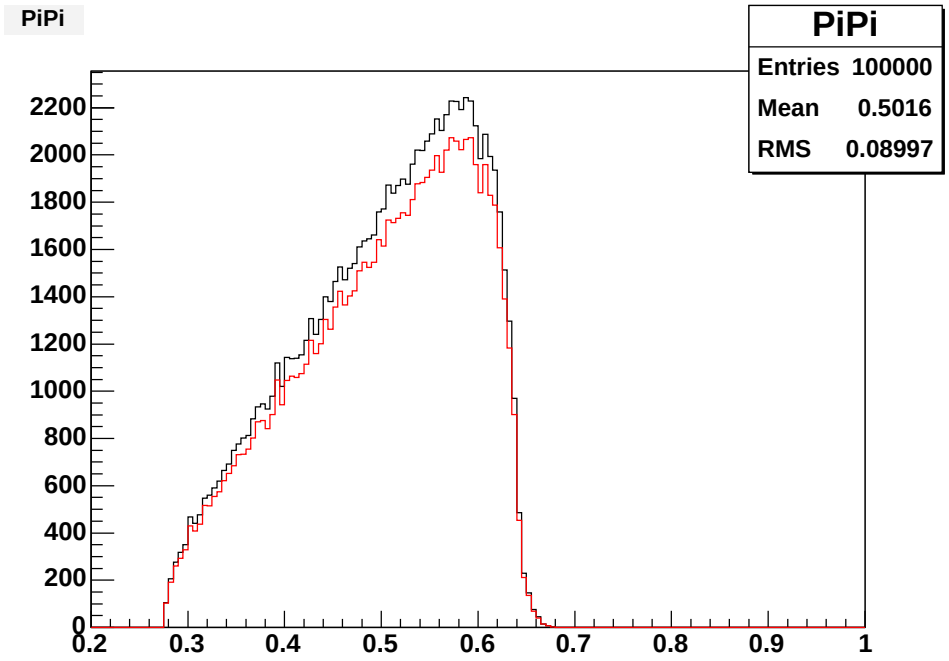

Fig. 24. Inv $\pi\pi$ mass for the two pions from the ρ decay in Reaction 6 (see Table 2). Black: generated, red: accepted events.

as a mean to decay the ω. Therefore for this reaction we have only two isobars (as compared to three in all the previous reactions), namely the b_1^+ and the

ω. This leads to only two reference frames in the PWA, the Gottfried-Jackson (GJ) frame and the helicity frame.

92 628 events were accepted after running the generated events through the geometrical detector simulation. This leads to a single-photon acceptance, A_γ, of

$$\begin{aligned} A_{\text{tot}} &= A_{\text{c}}^3 \cdot A_\gamma^4 \\ &= 0.92628 \\ \Rightarrow A_\gamma &= \sqrt[4]{\frac{0.92628}{A_{\text{c}}^3}} \\ &= 0.9841 \end{aligned}$$

where we have again used $A_{\text{c}} = 99.58$ % (see Table 4). The additional constraint for the minimum energy deposited in the BCAL and the LGD reduces the date set to 87 566 events and performing the elliptical cut shrinks the set to 86 030 events. Table 9 gives an overview over all the data sets and the calculated photon acceptances.

	# of events	A_{tot}	A_{c}	A_γ
Gen	100 000	100 %	100 %	100 %
Geo	92 628	92.63 %	99.58 %	98.41 %
minE	87 566	87.57 %	99.58 %	97.04 %
γSel	86 030	86.03 %	99.58 %	96.61 %

Table 9
Event totals and acceptance for Reaction 6 (see Table 2). Gen = generated events, Geo = after geometrical acceptance, minE = after minimum energy cut on photons detected in LGD and BCAL, γSel = elliptical cut on $\gamma\gamma$ masses.

11.2 Acceptance as a function of M_{tot}

The acceptance as a function of the total meson mass, M_{tot}, again shows a flat, structureless behavior over the peak of the $\pi_1(1700)$ resonance (see Fig. 25). The larger fluctuations in the regions below 1.5 GeV/c^2 and above 2.5 GeV/c^2 are again caused by lack of statistics.

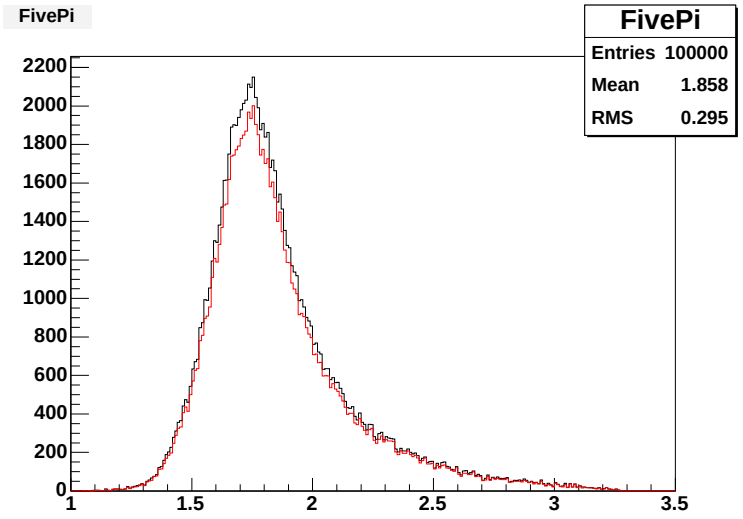

(a) M_{tot}. Black: generated, red: accepted events

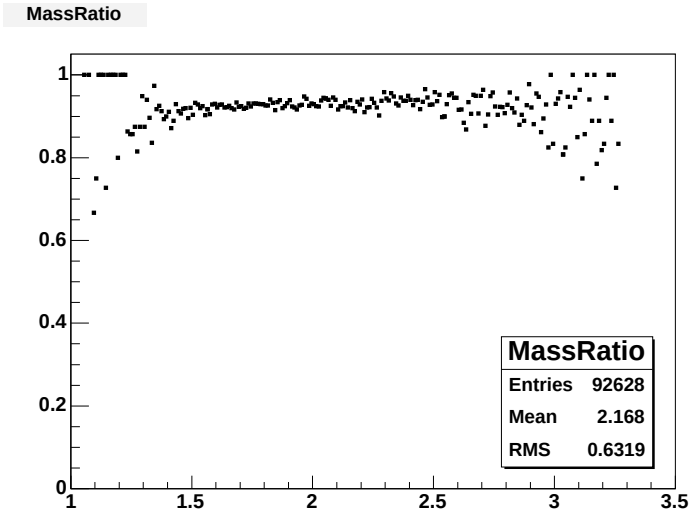

(b) Acceptance

Fig. 25. Acceptance as a function of M_{tot} for Reaction 6 (see Table 2).

11.3 Acceptance as a function of helicity angles

Fig. 26 shows the acceptance as a function of the angles used in the PWA for this reaction. Except for the $\cos(\theta_{GJ})$ distribution the curves again show no evident structure. Again, the loss of acceptance at $|\cos(\theta_{GJ})| \approx 1$ is expected since there is a π° recoiling against the $b_1(1235)$, causing the photons to go into the forward direction and being lost in the LGD beam hole.

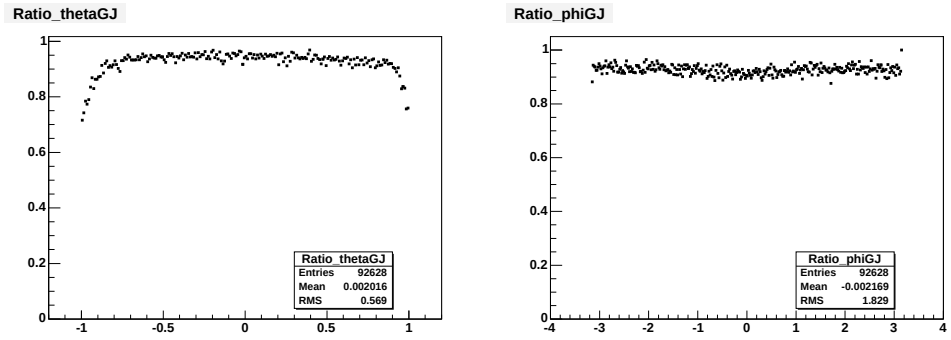

(a) $\cos(\theta_{GJ})$ (b) ϕ_{TY}

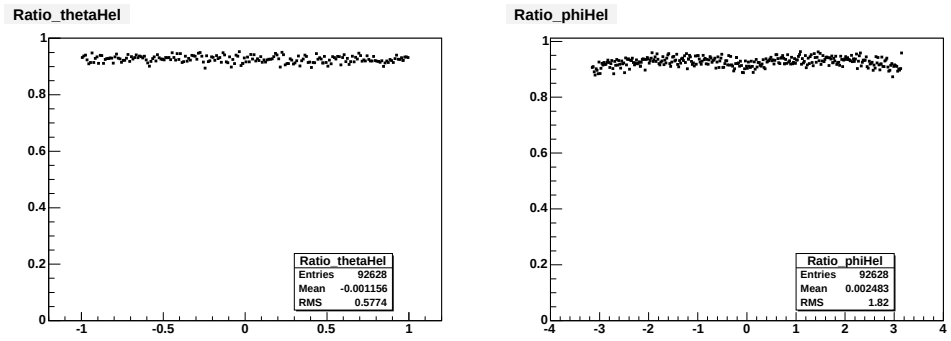

(c) $\cos(\theta^h)$ (d) ϕ^h

Fig. 26. Acceptance as a function of the various angles used in the PWA for Reaction 6 (see Table 2).

12 Results for $\gamma p \to h_2(2000)p \to \pi^+\pi^-\pi^+\pi^-2\gamma\ p$ (Reaction 7)

$$\begin{aligned}
\gamma p &\to h_2 p \\
h_2 &\to b_1^- \pi^+ \\
b_1^- &\to \omega\pi^- \\
\omega &\to \pi^+\pi^-\pi^\circ \ , \quad \pi^\circ \to \gamma\gamma
\end{aligned}$$

12.1 Accepted events totals

Again, this reaction contains the decay of an $\omega \to 3\pi$, which is treated the same way as in Section 11. Of the 100 000 events 95 223 were accepted after running the generated events through the detector geometrical simulation, leading to a single-photon acceptance A_γ of

$$\begin{aligned}
A_{\rm tot} &= A_{\rm c}^4 \cdot A_\gamma^2 \\
&= 0.95223 \\
\Rightarrow A_\gamma &= \sqrt{\frac{0.95223}{A_{\rm c}^4}} \\
&= 0.9841
\end{aligned}$$

where we have again used $A_{\rm c} = 99.58$ % (see Table 4). The additional constraint for the minimum energy deposited in the BCAL and the LGD reduces the date set to 92 386 events. Table 10 gives an overview over all the data sets and the calculated photon acceptances.

	# of events	$A_{\rm tot}$	$A_{\rm c}$	A_γ
Gen	100 000	100 %	100 %	100 %
Geo	95 223	95.22 %	99.58 %	98.41 %
minE	92 386	92.39 %	99.58 %	96.93 %
γSel	N/A			

Table 10
Event totals and acceptance for Reaction 7 (see Table 2). Gen = generated events, Geo = after geometrical acceptance, minE = after minimum energy cut on photons detected in LGD and BCAL, γSel = elliptical cut on $\gamma\gamma$ masses.

12.2 Acceptance as a function of M_{tot}

The acceptance as a function of the total meson mass, M_{tot}, is again structureless and smooth over the peak of the $h_2(2000)$. The large variations at low and high masses are due to lack of statistics in these regions.

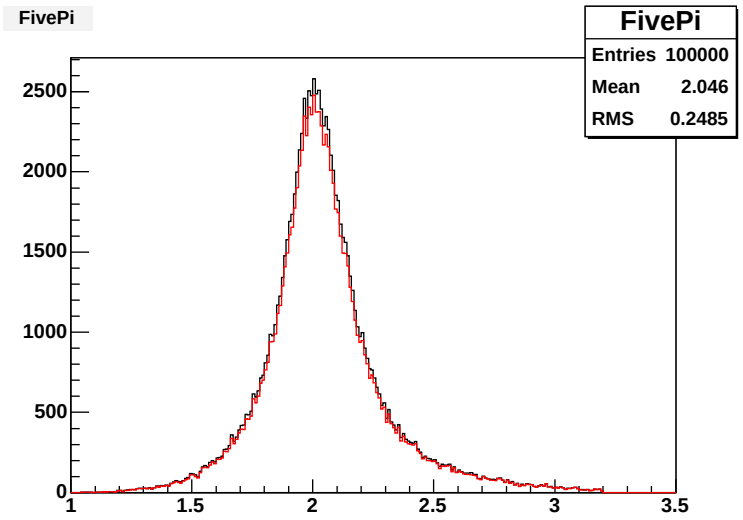

(a) M_{tot}. Black: generated, red: accepted events

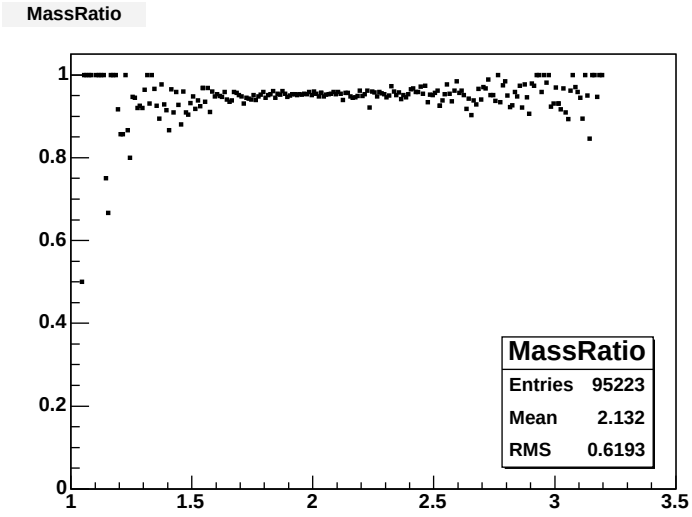

(b) Acceptance

Fig. 27. Acceptance as a function of M_{tot} for Reaction 7 (see Table 2).

12.3 Acceptance as a function of helicity angles

Fig. 28 shows the acceptance as a function of the angles used in the PWA for this reaction. The distributions again show the expected behavior, caused by the π^+, recoiling against the $b_1^-(1235)$, escaping detection through the beam hole in the forward drift chambers.

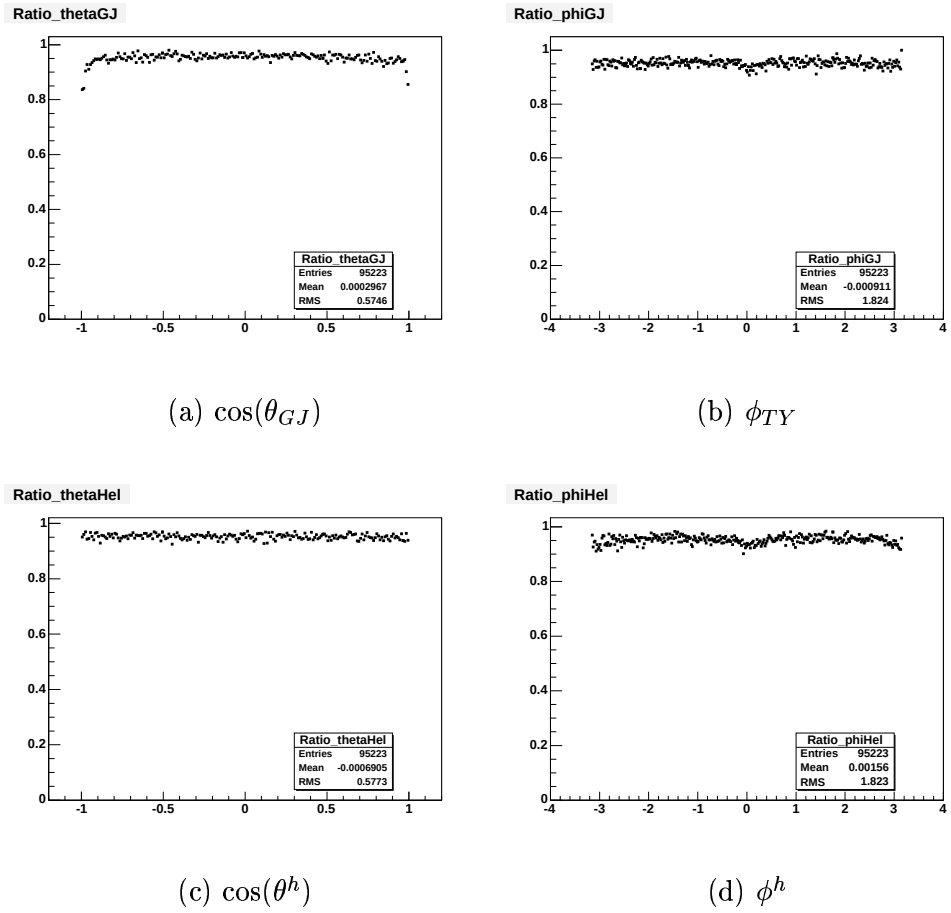

(a) $\cos(\theta_{GJ})$ (b) ϕ_{TY}

(c) $\cos(\theta^h)$ (d) ϕ^h

Fig. 28. Acceptance as a function of the various angles used in the PWA for Reaction 7 (see Table 2).

13 Conclusions

We have carried out an acceptance study for the GlueX detector system. The acceptance as a function of helicity angles was determined for several reactions involving expected and observed masses for exotic meson resonances, the detection of which is one the main goals of the experiment. It was found that the acceptance in general is flat and rather high, depending only on the observed final state particles. For charged π we found a geometrical acceptance of $A_c > 99\%$, with losses mostly due to the forward beam hole in the FDCs ($\theta_{\pi^\pm}^{\mathrm{Lab}} \lesssim 1^\circ$). For photons the acceptance is $A_\gamma \approx 96.5\%$, after several simple cuts to simulate reconstruction into neutral final state mesons. Geometrical losses occur in the forward direction ($\theta_\gamma^{\mathrm{Lab}} \lesssim 1^\circ$), due to the beam hole in the LGD, and in the backward direction ($\theta_\gamma^{\mathrm{Lab}} \gtrsim 130^\circ$), because BCAL covers detection only up to this angle.

A slight loss of acceptance was observed as a function of $\cos(\theta_{GJ})$, due to the recoil meson from the decay of the generated resonance being lost in the very forward detection, where particles are undetectable due to holes in the detectors. This behavior is observed for both, neutral and charged mesons recoiling against the primary isobar, since both, drift chambers, detecting charged mesons, and the LGD, detecting forward-going photons from the decay of neutral mesons, have an uninstrumented section in order to let beam particles that do not interact in the target pass through the detector systems undetected. Since the loss of events does not cause a sharp change in the acceptance, this drop should be easily correctable in a PWA and will likely not cause major difficulties.

Appendix

A GlueX calorimetry

A.1 Geometry

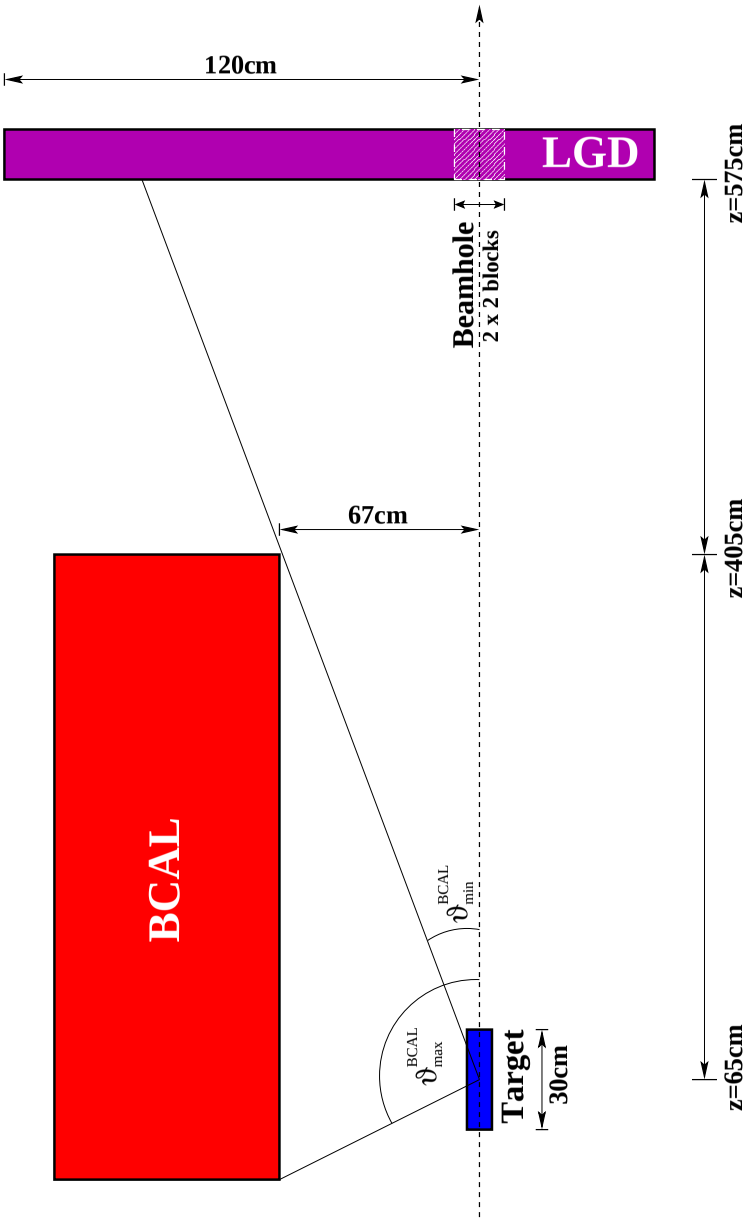

Fig. A.1. Geometry of the GlueX calorimeters.

Fig. A.1 shows that the BCAL has a total length of 390 cm, with the downstream end at $z = 405$ cm. With the inner radius of the BCAL equal to 67 cm and the 15 cm long target centered at $z = 65$ cm one gets

$$\begin{aligned} \theta_{\min}^{\mathrm{BCAL}} &= \arctan\left(\frac{67\ \mathrm{cm}}{340\ \mathrm{cm}}\right) = 11.15^{\circ} \\ \theta_{\max}^{\mathrm{BCAL}} &= 180^{\circ} - \arctan\left(\frac{67\ \mathrm{cm}}{50\ \mathrm{cm}}\right) = 126.73^{\circ} \end{aligned} \tag{A.1}$$

In the simulation code the LGD array is assumed to be circular, even though in reality it will be assembled from lead glass blocks with a square, 4 cm×4 cm, front surface. Since the photons that are detected in the BCAL will be lost for detection in the LGD the exact outer shape of the LGD may not play an important role as long as there is a sufficient overlap (i.e. no gaps) between the two calorimeters. With a radius of 120 cm and the front face of the LGD at $z = 575$ cm the maximum angle for a photon detected in the LGD is

$$\theta_{\max}^{\mathrm{LGD}} = \arctan\left(\frac{120\ \mathrm{cm}}{510\ \mathrm{cm}}\right) = 13.24^{\circ}, \tag{A.2}$$

which will provide enough overlap between the two detectors.

As already mentioned the LGD has a small hole in the center in order to let non-interacting beam particles pass through the detector. This causes a small gap in the acceptance at small angles. The beam hole has a square shape and a size of 2×2 lead glass blocks (8 cm × 8 cm). This leads to a minimum angle for LGD photons of

$$\begin{aligned} \theta_{\min}^{\mathrm{LGD}} &= \arctan\left(\frac{4\ \mathrm{cm}}{510\ \mathrm{cm}}\right) = 0.45^{\circ} \quad \text{or} \\ \theta_{\min}^{\mathrm{LGD}} &= \arctan\left(\frac{\sqrt{4^2+4^2}\ \mathrm{cm}}{510\ \mathrm{cm}}\right) = 0.64^{\circ}, \end{aligned} \tag{A.3}$$

where the first value is in the x- or y-direction and the second value in the diagonal. With this configuration the acceptance for photons in the detector

is (see Fig. A.2)

$$\begin{aligned} A_{\text{tot}} = A_\gamma^8 &= \frac{93\,575}{100\,000} \\ \Rightarrow A_\gamma &= \sqrt[8]{0.93575} \\ &= 0.9917 \end{aligned}$$

Normally photons hitting any of the innermost crystals, surrounding the beam hole are rejected, since these photons would not deposit all their energy and would therefore be rather difficult to reconstruct. For this reason another layer of crystals around the beam hole is discarded in the simulation. This leads to a 4×4 lead glass blocks (16 cm $\times$ 16 cm) beam hole and minimum angles of

$$\begin{aligned} \theta_{\text{min}}^{\text{LGD}} &= \arctan\left(\frac{8\text{ cm}}{510\text{ cm}}\right) = 0.90^\circ \quad \text{or} \\ \theta_{\text{min}}^{\text{LGD}} &= \arctan\left(\frac{\sqrt{8^2+8^2}\text{ cm}}{510\text{ cm}}\right) = 1.27^\circ. \end{aligned} \tag{A.4}$$

The effect of the 16 cm $\times$ 16 cm beam hole on the photon acceptance is shown in Fig. A.3. The larger beam hole clearly results in a drop of the acceptance at very small angles as compared to the 8 cm $\times$ 8 cm beam hole (Fig. A.2). The acceptance for photons drops to

$$\begin{aligned} A_{\text{tot}} = A_\gamma^8 &= \frac{90\,016}{100\,000} \\ \Rightarrow A_\gamma &= \sqrt[8]{0.90016} \\ &= 0.9869 \end{aligned}$$

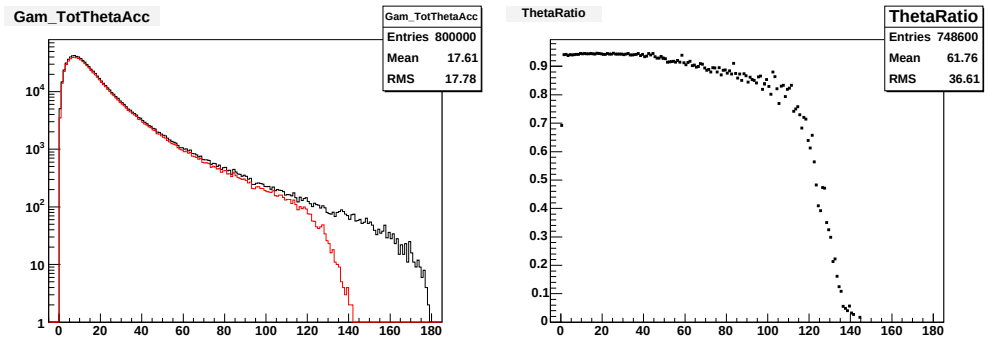

Fig. A.2. Acceptance as a function of the polar angle in the lab frame, $\theta_\gamma^{\mathrm{Lab}}$ for all photons from Reaction 3 (see Table 2). For this simulation the LGD beam hole had a size of 8 cm $\times$ 8 cm. (a) Number of events as a function of $\theta_\gamma^{\mathrm{Lab}}$ (black: generated events, red: accepted events) (b) Acceptance as a function of $\theta_\gamma^{\mathrm{Lab}}$.

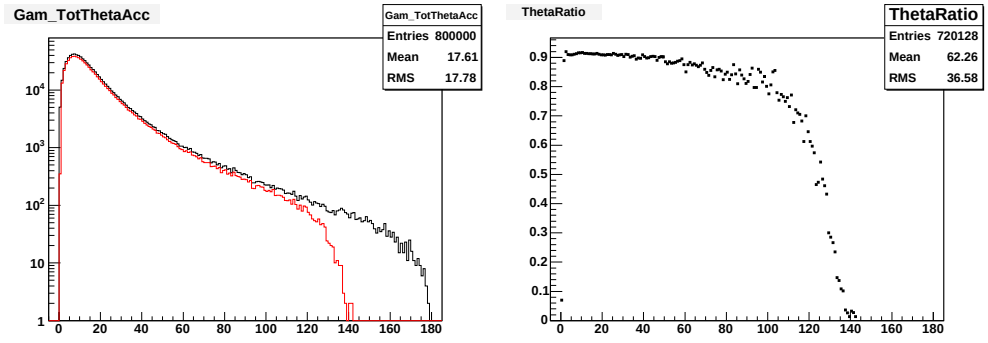

Fig. A.3. Acceptance as a function of the polar angle in the lab frame, $\theta_\gamma^{\mathrm{Lab}}$ for all photons from Reaction 3 (see Table 2). For this simulation the LGD beam hole had a size of 16 cm $\times$ 16 cm. (a) Number of events as a function of $\theta_\gamma^{\mathrm{Lab}}$ (black: generated events, red: accepted events) (b) Acceptance as a function of $\theta_\gamma^{\mathrm{Lab}}$.

B Effect on acceptance due to non-hermetic calorimetry

B.1 Geometry

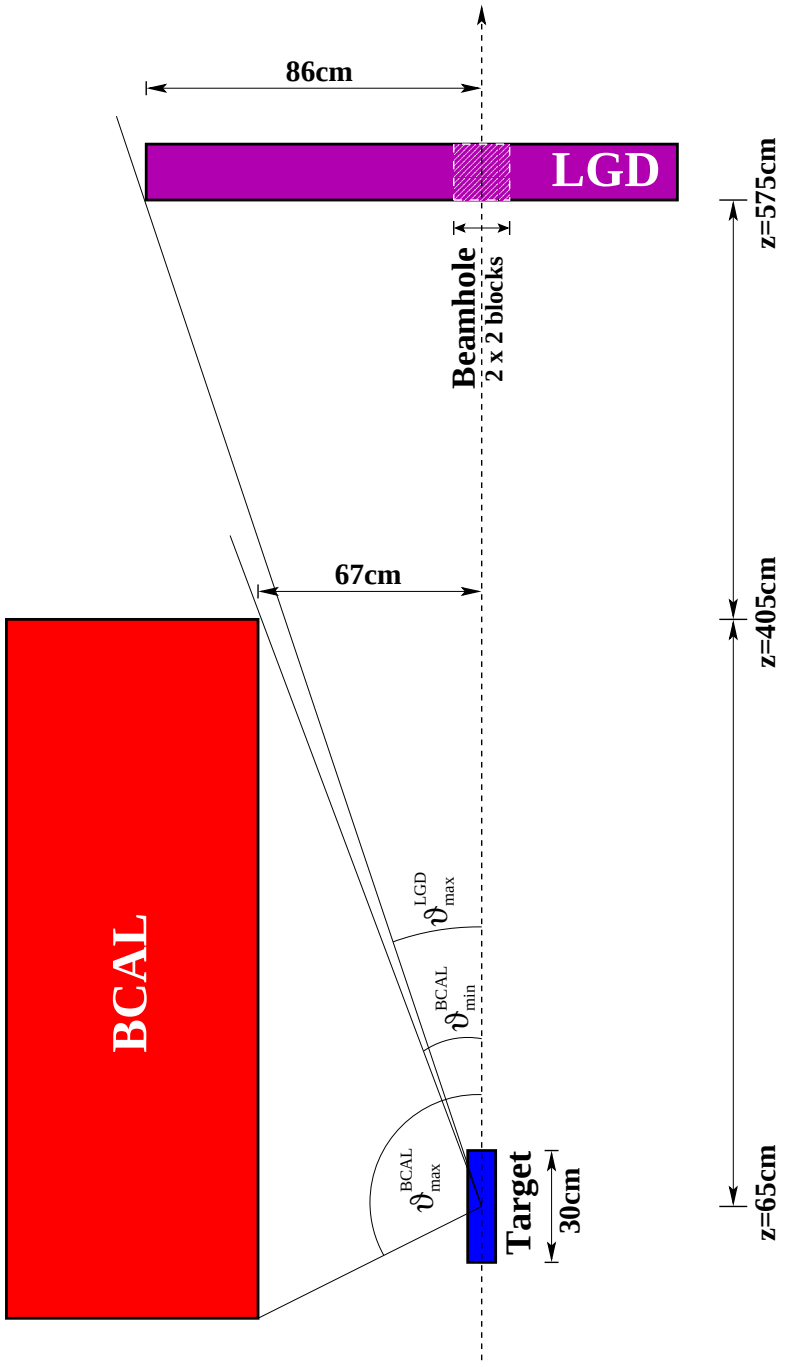

Fig. B.1. Geometry of the GlueX calorimeters.

B.2 Geometrical limits of the calorimeters

Using the setup shown in Fig. B.1, where the LGD was only 86 cm long and located at $z = 575$ cm one gets for the maximum angle for photons to be detected in the LGD

$$\theta_{\text{max}}^{\text{LGD}} = \arctan\left(\frac{86 \text{ cm}}{510 \text{ cm}}\right) = 9.57^{\circ}, \tag{B.1}$$

whereas the minimum angle for photons to be detected in the BCAL (located at $z = 405$ cm and minimum radius of 67 cm) is

$$\theta_{\text{min}}^{\text{BCAL}} = \arctan\left(\frac{67 \text{ cm}}{340 \text{ cm}}\right) = 11.15^{\circ}. \tag{B.2}$$

This setup creates a gap of $\Delta\theta \approx 1.5^{\circ}$ between the two calorimeters.

B.3 Acceptance distributions

In what follows we have used the all neutral data set from Reaction 3 (see Table 2), unless otherwise noted. The reaction has 8 photons in the final state from the decay of 4 neutral mesons

$$\begin{aligned}
&\gamma p \to \pi_1^{\circ} p \\
&\qquad \pi_1^{\circ} \to f_1 \pi^{\circ}\,, \;\; \pi^{\circ} \to \gamma\gamma \\
&\qquad\qquad f_1 \to a_0^{\circ}\pi^{\circ} \quad , \quad \pi^{\circ} \to \gamma\gamma \\
&\qquad\qquad\qquad a_0^{\circ} \to \pi^{\circ}\eta \quad , \quad \pi^{\circ}, \eta \to \gamma\gamma
\end{aligned}$$

With 67 401 accepted events after the detector simulation `HDFast`, the acceptance for photons drops from $A_{\gamma} = 99.17$ % (see section 8.1) to

$$\begin{aligned}
A_{\text{tot}} &= A_{\gamma}^{8} \\
&= 0.67401 \\
\Rightarrow A_{\gamma} &= \sqrt[8]{0.67401} \\
&= 95.19 \text{ \%}
\end{aligned}$$

Fig. B.2 shows the acceptance as a function of the laboratory angle $\theta_{\gamma}^{\text{Lab}}$ for photons from the decay of neutral π and η. As can be seen, besides the beam hole (at $\theta_{\gamma}^{\text{Lab}} < 1^{\circ}$) and the maximum BCAL angle ($\theta_{\gamma}^{\text{Lab}} \approx 130^{\circ}$) the gap between the detectors at $\theta_{\gamma}^{\text{Lab}} \approx 11^{\circ}$ is clearly visible as well.

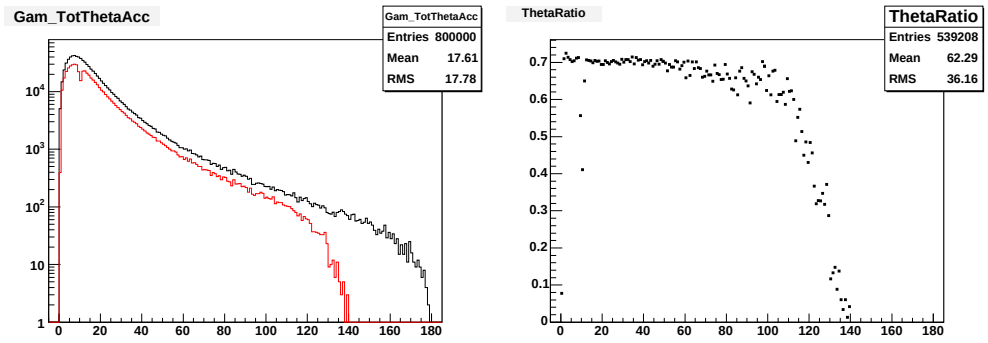

Fig. B.2. Acceptance as a function of the polar angle in the lab frame, $\theta_\gamma^{\mathrm{Lab}}$ for all photons with a non-hermetic calorimetry setup. (a) Number of events as a function of $\theta_\gamma^{\mathrm{Lab}}$ (black: generated events, red: accepted events) (b) Acceptance as a function of $\theta_\gamma^{\mathrm{Lab}}$.

The acceptance as a function of the helicity angles is shown in Fig. B.3. With the exception of the $\cos(\theta_{GJ})$ distribution (Fig. B.3(a)) the curves show no structures over the range of each angle. The depletion of the acceptance at $\cos(\theta_{GJ}) \approx -0.3$ is caused by the strong correlation between $\cos(\theta_{GJ})$ and $\theta_\gamma^{\mathrm{Lab}}$, the polar angle in the laboratory frame, for photons from the decay of the recoil to the first isobar (in this reaction $f_1(1285)$). This is evident from Fig. B.4 which shows $\cos(\theta_{GJ})$ vs $\theta_\gamma^{\mathrm{Lab}}$ for the 8 photons in the reaction from generated events. The two right plots in the bottom row are for the photons from the decay of the $\pi^\circ \to \gamma\gamma$ recoil to the $f_1(1285)$. Restricting $\theta_\gamma^{\mathrm{Lab}}$ to the range $10^\circ < \theta_\gamma^{\mathrm{Lab}} < 12^\circ$, which simulates the drop in photon acceptance at $\theta_\gamma^{\mathrm{Lab}} \approx 11^\circ$ (see Fig. B.2), shows that for the two photons from the decay of the recoil π° the $\cos(\theta_{GJ})$ is strongly peaked around a value of ≈ -0.3 (see right two plots in the bottom row of Fig. B.5). The drop of acceptance is also evident from the distribution of $\cos(\theta_{GJ})$ vs $\theta_\gamma^{\mathrm{Lab}}$ for accepted events (Fig. B.6).

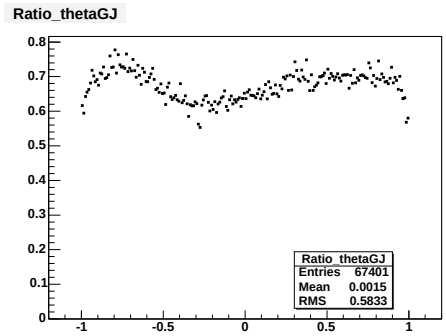

(a) $\cos(\theta_{GJ})$

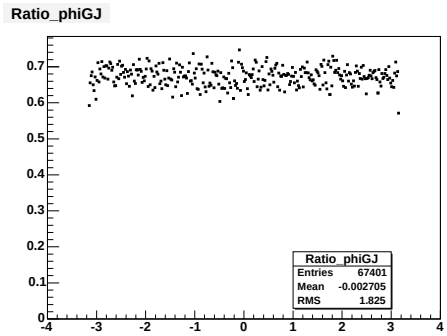

(b) ϕ_{TY}

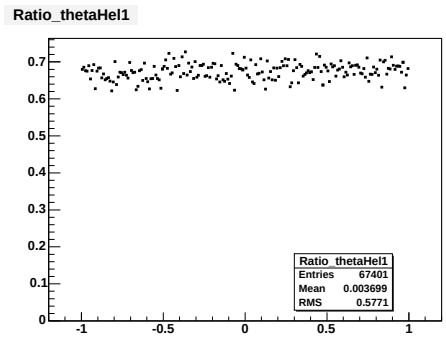

(c) $\cos(\theta_1^h)$

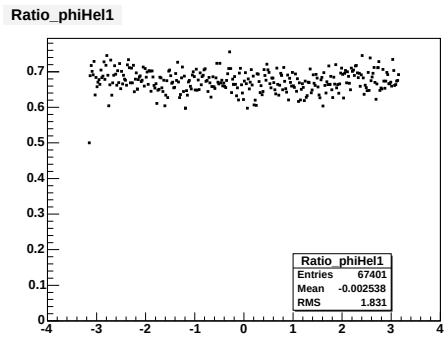

(d) ϕ_1^h

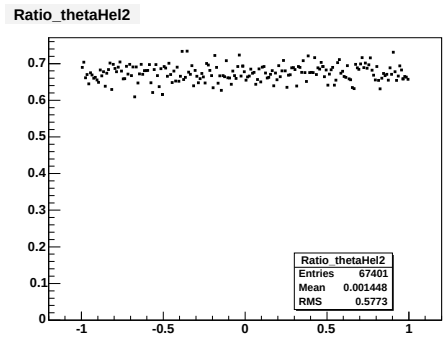

(e) $\cos(\theta_2^h)$

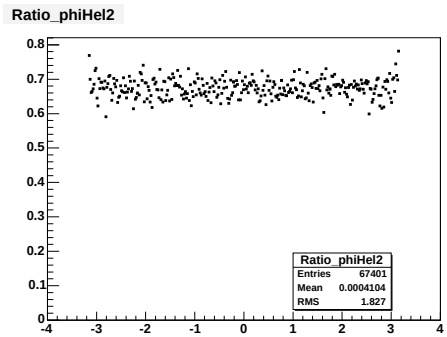

(f) ϕ_2^h

Fig. B.3. Acceptance as a function of the various angles used in the PWA with a non-hermetic calorimetry setup.

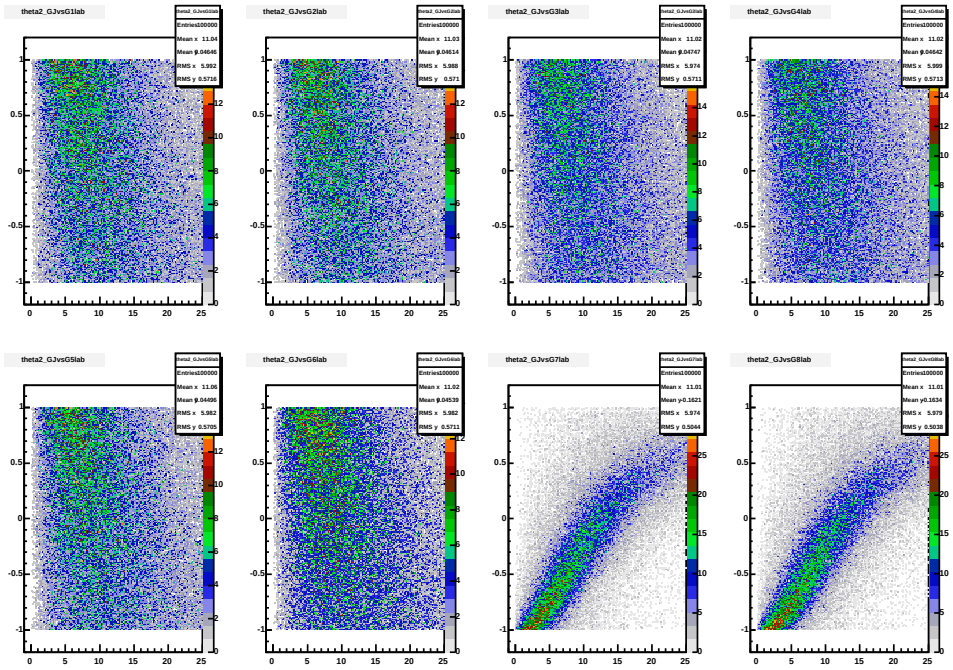

Fig. B.4. $\cos(\theta_{GJ})$ vs $\theta_{\gamma}^{\mathrm{Lab}}$ for the 8 photons from the generated data set.

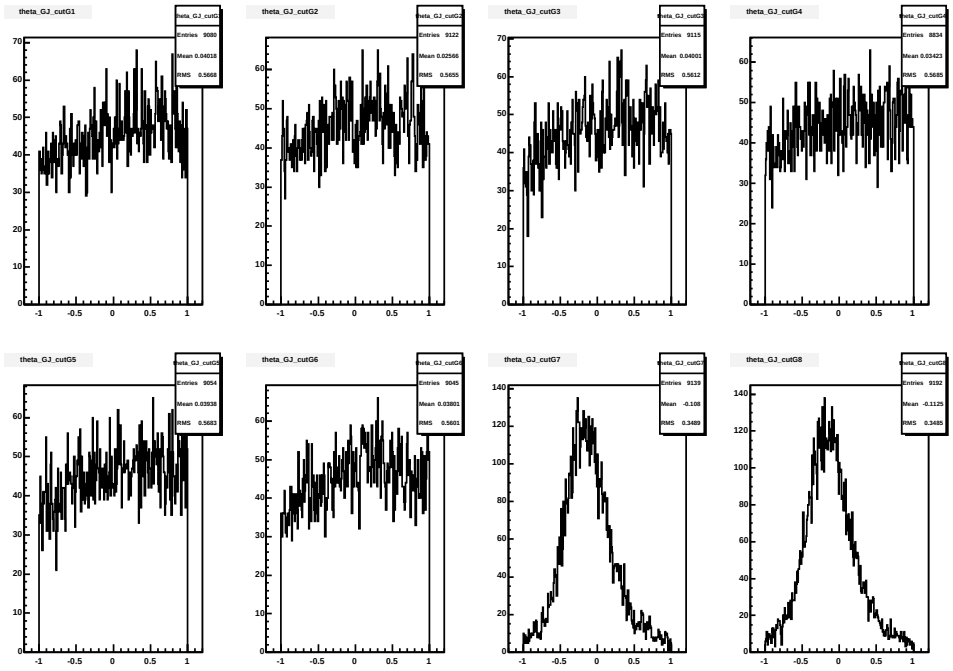

Fig. B.5. $\cos(\theta_{GJ})$ distributions with a cut $10^{\circ} < \theta_{\gamma}^{\mathrm{Lab}} < 12^{\circ}$.

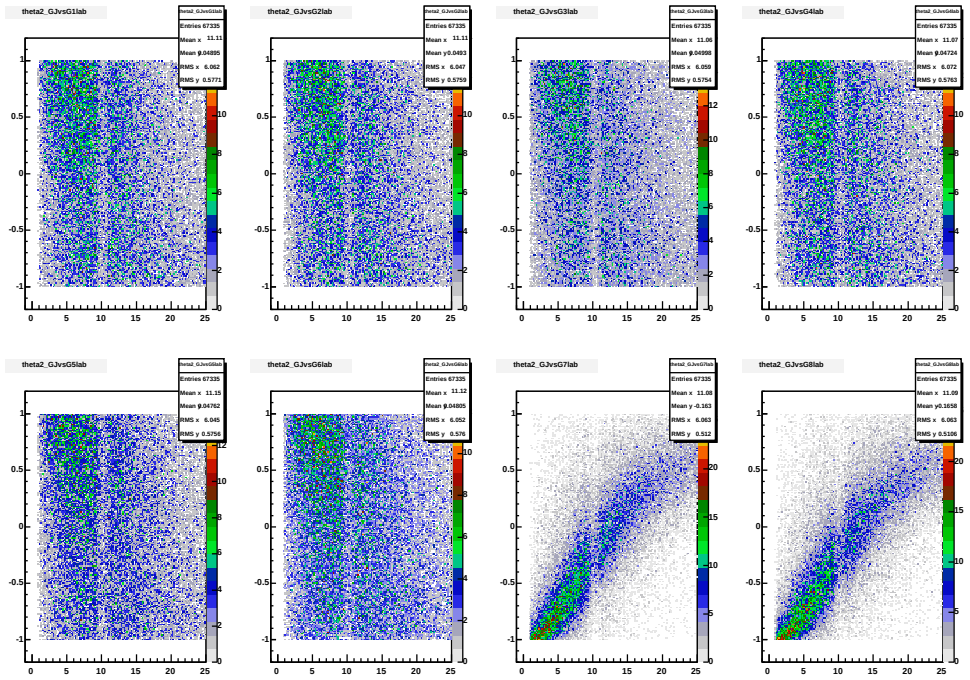

Fig. B.6. $\cos(\theta_{GJ})$ vs $\theta_{\gamma}^{\mathrm{Lab}}$ for the 8 photons from the accepted data set (after the detector simulation `HDFast`).

The effect should also appears for other final states. Fig B.7 shows the acceptance as a function of $\cos(\theta_{GJ})$ for the reaction

$$\begin{aligned}
&\gamma p \to \pi_1^\circ p \\
&\qquad \pi_1^\circ \to a_1^\circ \eta \quad , \ \eta \to \gamma\gamma \\
&\qquad\qquad a_1^\circ \to \rho^+ \pi^- \\
&\qquad\qquad\qquad \rho^+ \to \pi^+ \pi^\circ \, , \quad \pi^\circ \to \gamma\gamma
\end{aligned}$$

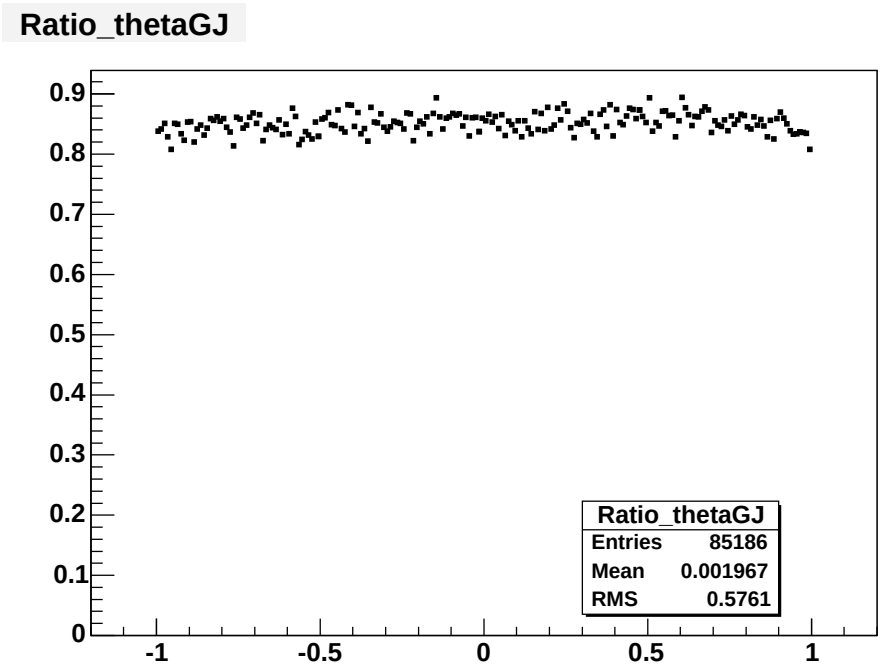

Fig. B.7. Acceptance as a function $\cos(\theta_{GJ})$ for the Reaction 4 (see Table 2) with non-hermetic calorimetry setup.

It is surprising that here we do not seem to observe the dip in the acceptance for $\cos(\theta_{GJ})$ as in Fig. B.3(a). The reason for this is that in this case the recoil to the primary isobar is an $\eta \to \gamma\gamma$, which is much heavier than the π° in the previous reaction and therefore the correlation between $\cos(\theta_{GJ})$ and $\theta_\gamma^{\rm Lab}$ is not as strong. The drop in acceptance is still present, but is hidden. This is illustrated in Figs. B.8 to B.10, where the bottom rows are the distributions from the photons of the decay $\eta \to \gamma\gamma$.

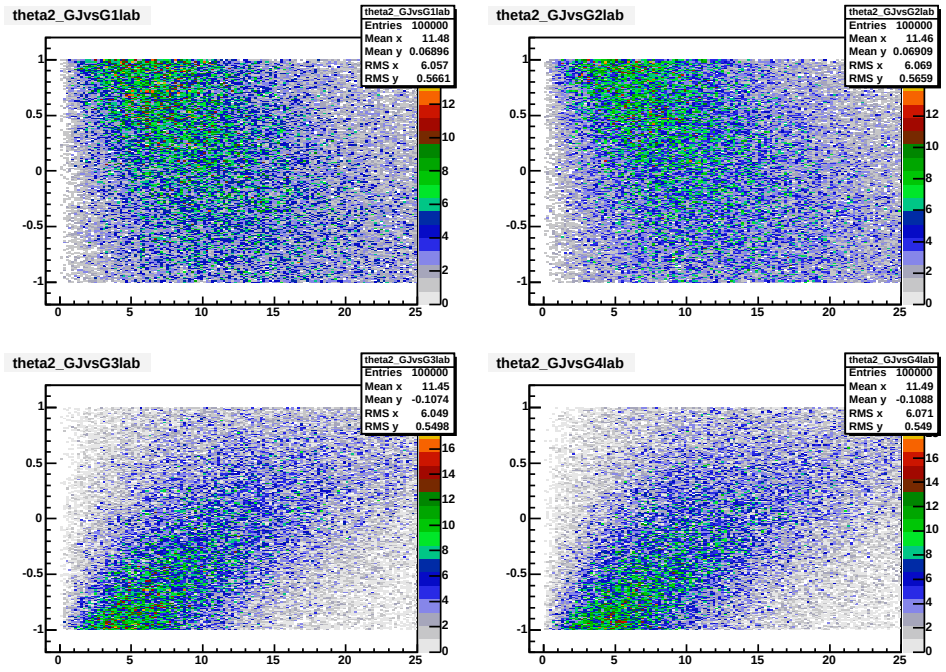

Fig. B.8. $\cos(\theta_{GJ})$ vs $\theta_{\gamma}^{\mathrm{Lab}}$ for the 4 photons from the generated data set of Reaction 4 (see Table 2).

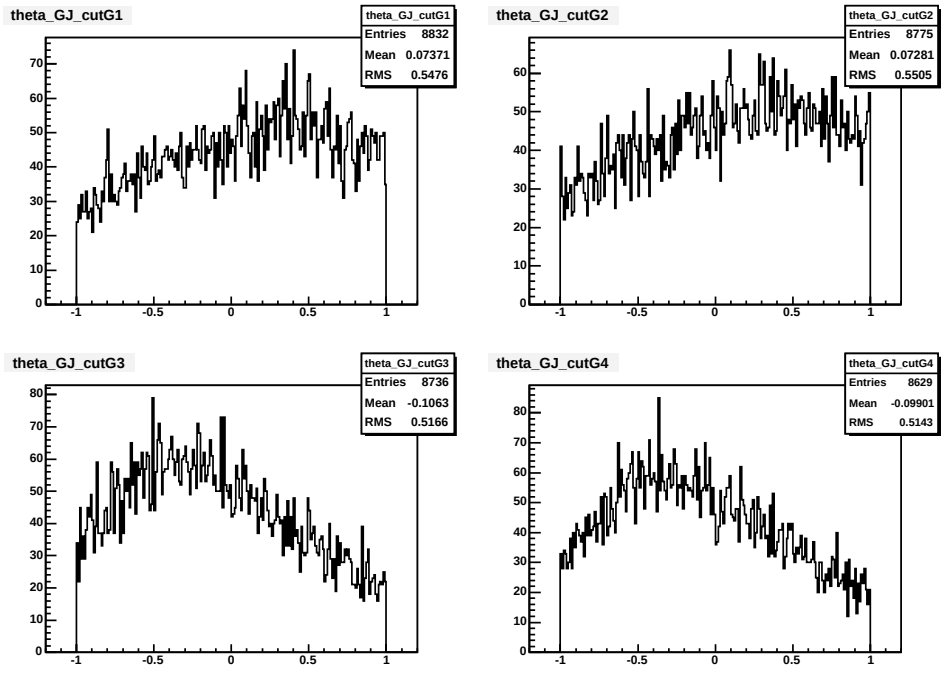

Fig. B.9. $\cos(\theta_{GJ})$ distributions with a cut $10^{\circ} < \theta_{\gamma}^{\mathrm{Lab}} < 12^{\circ}$.

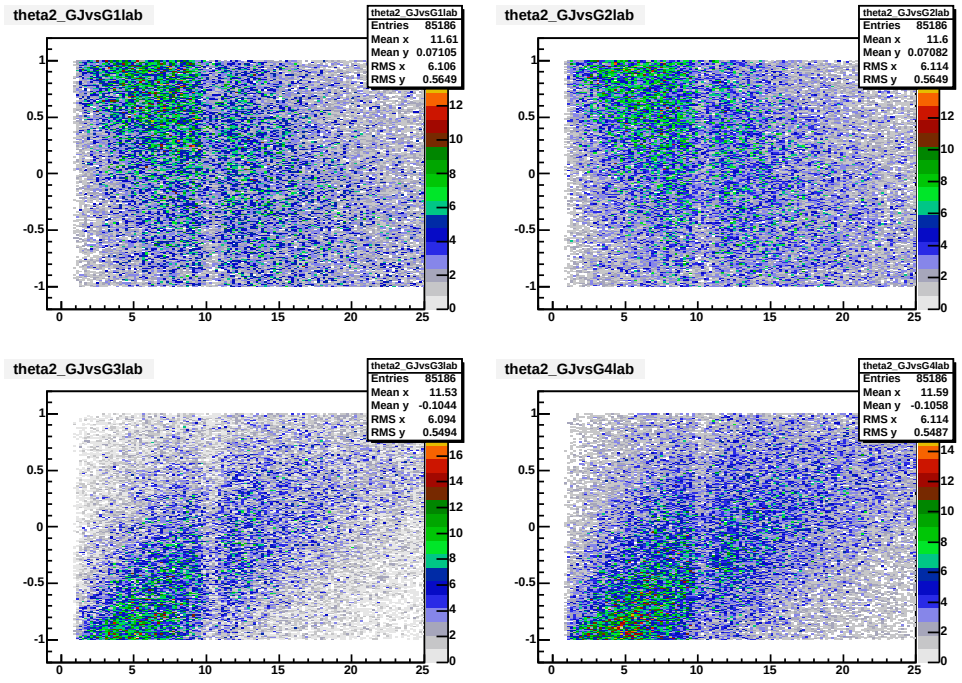

Fig. B.10. $\cos(\theta_{GJ})$ vs $\theta_{\gamma}^{\mathrm{Lab}}$ for the 4 photons from the accepted data set of Reaction 4 (see Table 2).

B.4 Mass dependence of the effect

We also carried out a study to investigate the dependence of the drop in $\cos(\theta_{GJ})$ acceptance on the mass of the produced resonance. For this study we again considered the all-neutral reaction

$$\gamma p \to \pi_1^\circ p \to f_1(1285)\pi^\circ p \to [a_0^\circ(980)\pi^\circ]\pi^\circ p \to [\pi^\circ\eta\pi^\circ]\pi^\circ p \tag{B.3}$$

with three values for the mass of the π_1°

1. $M_X = 1300$ MeV/c^2
2. $M_X = 1700$ MeV/c^2
3. $M_X = 2400$ MeV/c^2

The correlation between the photons from the π° decay and $\cos(\theta_{GJ})$ is demonstrated in Fig. B.11. For one of the two photons from $\pi^\circ \to \gamma\gamma$ we again performed a cut to "simulate" the drop in photon acceptance around $\theta_\gamma^{\text{Lab}} \approx 11^\circ$

$$10^\circ < \theta_\gamma^{\text{Lab}} < 12^\circ \tag{B.4}$$

For events inside this cut Fig. B.11 shows the distribution of $\cos(\theta_{GJ})$ for the three different data sets. It is evident that for the high-mas state ($M_X = 2400$ MeV/c^2) the distribution of $\cos(\theta_{GJ})$ becomes narrower and shifts toward lower values of $\cos(\theta_{GJ})$. We therefore expect that the depletion in the acceptance as a function of $\cos(\theta_{GJ})$ will be more localized. This is confirmed in Fig. B.12.

There is no noticeable difference between the other two generated data sets at $M_X = 1300$ MeV/c^2 and $M_X = 1700$ MeV/c^2.

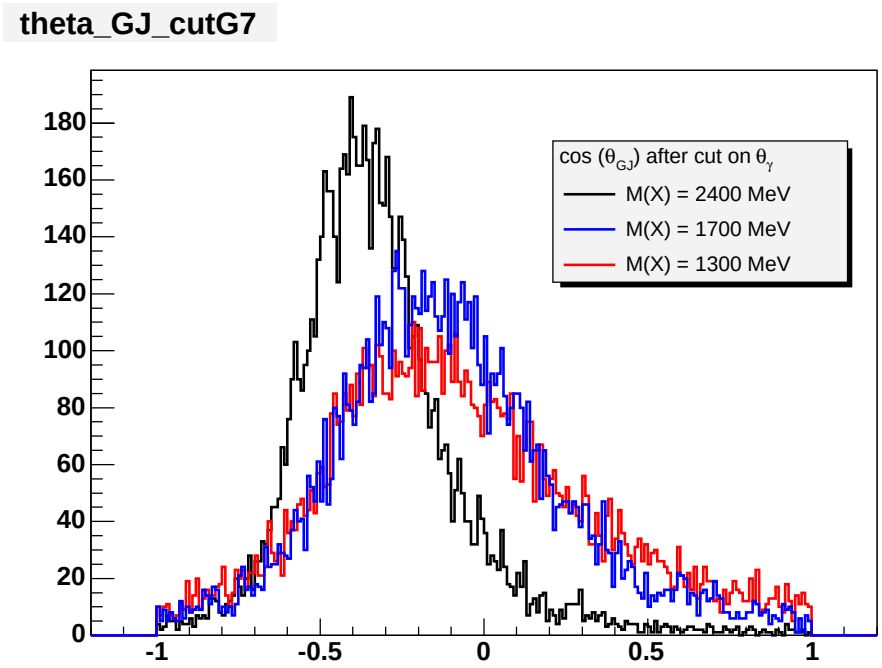

Fig. B.11. $\cos(\theta_{GJ})$ with a cut $10^\circ < \theta_\gamma^{\mathrm{Lab}} < 12^\circ$ for one of the two photons from the decay of the recoil $\pi^\circ \to \gamma\gamma$.

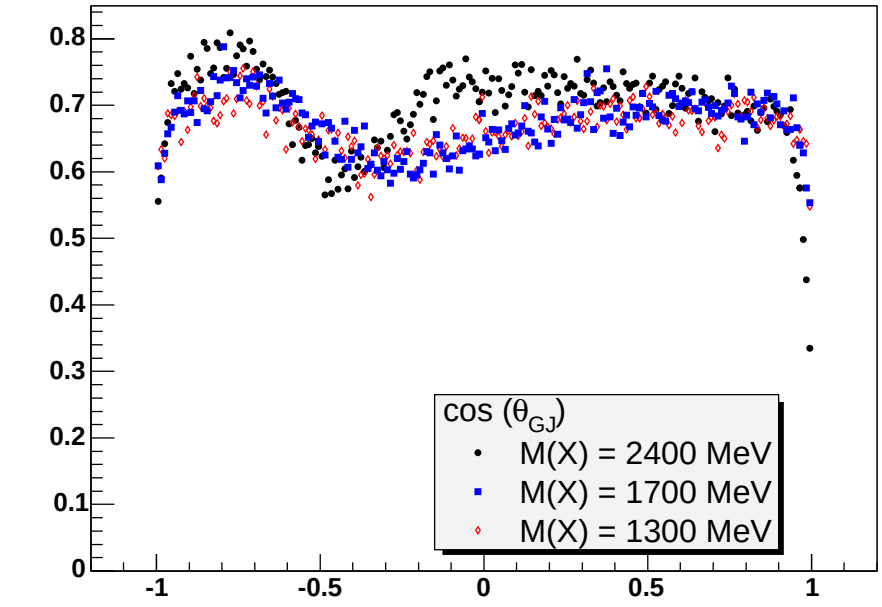

Fig. B.12. Acceptance as a function of $\cos(\theta_{GJ})$

References

[1] P. E. Eugenio, A general monte carlo event generator, gluex-doc-11, Carnegie Mellon University (1998).

[2] P. Page, E. S. Swanson, A. P. Szczepaniak, Phys. Rev. D59 (1999) 034016.